Dissociable encoding of motivated behavior by parallel thalamo-striatal projections

Sofia Beas[1,2#], Isbah Khan[1], Claire Gao[1], Gabriel Loewinger[3], Emma Macdonald[1], Alison Bashford[1], Shakira Rodriguez-Gonzalez[1], Francisco Pereira[3], Mario A. Penzo[1#]

1 – Unit on the Neurobiology of Affective Memory, National Institute of Mental Health, Bethesda, MD, USA.

2 – Department of Neurobiology, University of Alabama at Birmingham, Birmingham, AL, USA.

3 – Machine Learning Team, National Institute of Mental Health, Bethesda, MD, USA.

[#] Correspondence: Sofia Beas, Ph.D. Email: sbeas@uab.edu ; Mario A. Penzo, Ph.D. Email: mario.penzo@nih.gov

SUMMARY

The successful pursuit of goals requires the coordinated execution and termination of actions that lead to positive outcomes. This process is thought to rely on motivational states that are guided by internal drivers, such as hunger or fear. However, the mechanisms by which the brain tracks motivational states to shape instrumental actions are not fully understood. The paraventricular nucleus of the thalamus (PVT) is a midline thalamic nucleus that shapes motivated behaviors via its projections to the nucleus accumbens (NAc)[1-8] and monitors internal state via interoceptive inputs from the hypothalamus and brainstem[3,9-14]. Recent studies indicate that the PVT can be

21 subdivided into two major neuronal subpopulations, namely $PVT^{D2(+)}$ and $PVT^{D2(-)}$, which
22 differ in genetic identity, functionality, and anatomical connectivity to other brain regions,
23 including the NAc[4,15,16]. In this study, we used fiber photometry to investigate the *in vivo*
24 dynamics of these two distinct PVT neuronal types in mice performing a reward foraging-
25 like behavioral task. We discovered that $PVT^{D2(+)}$ and $PVT^{D2(-)}$ neurons encode the
26 execution and termination of goal-oriented actions, respectively. Furthermore, activity in
27 the $PVT^{D2(+)}$ neuronal population mirrored motivation parameters such as vigor and
28 satiety. Similarly, $PVT^{D2(-)}$ neurons, also mirrored some of these parameters but to a much
29 lesser extent. Importantly, these features were largely preserved when activity in PVT
30 projections to the NAc was selectively assessed. Collectively, our results highlight the
31 existence of two parallel thalamo-striatal projections that participate in the dynamic
32 regulation of goal pursuits and provide insight into the mechanisms by which the brain
33 tracks motivational states to shape instrumental actions.

34

35 **RESULTS**

36 **Characterization of motivated behavior in rodents using a foraging-like task**

37 Goal-oriented behaviors are generated by cortico-mesolimbic circuits that establish goal
38 objects based on need states, as well as the actions required to obtain those objects[17].
39 Recent reports suggest that the PVT plays a critical role in translating needs states into
40 motivation, owing to its strong innervation by the hypothalamus and brainstem[10,11,13,14,18].
41 The PVT is composed of molecularly diverse neuronal subpopulations that segregate
42 across the anteroposterior axis of the thalamus and project to the NAc[8,15,16,19].

43 Particularly, the PVT contains two major distinct subpopulations, termed $PVT^{D2(+)}$ and
44 $PVT^{D2(-)}$, respectively, identified based on the expression of the dopamine D2 receptor,
45 or lack thereof[4,16]. However, how activity within parallel thalamo-striatal projections arising
46 in the PVT relates to specific aspects of motivated behaviors remains unclear.

47 To address this question, we investigated the *in vivo* dynamics of $PVT^{D2(+)}$ and $PVT^{D2(-)}$
48 neurons using a reward foraging-like behavioral task[11,20]. In this task, mice initiated
49 individual trials by entering the "trigger zone" where they were presented with a cue that
50 signaled reward availability. Upon cue presentation, mice were required to traverse a long
51 corridor and reach the "reward zone" to obtain a food reward (Supp. Fig. 1A) (See
52 Methods). We found that mice successfully learned to shuttle back and forth to obtain the
53 food reward and were highly engaged in the task, as demonstrated by two observations.
54 First, they completed a significantly larger volume of trials in late compared to early
55 sessions (Supp. Fig. 1B). Second, they displayed shorter latencies to reach the reward
56 zone (Supp. Fig. 1C), obtain the reward (Supp. Fig. 1D), and initiate subsequent trials
57 (Supp. Fig. 1E).

58 We noticed that mice varied in latencies to perform individual trials, but after training, they
59 completed most trials under 11 seconds (~ 75% of completed trials; Supp. Fig. 1F). Thus,
60 trial engagement was denoted by trials completed in 11 seconds or less. As such, to
61 investigate how molecularly distinct subpopulations of the PVT encode various
62 parameters associated with goal pursuit, the analysis of calcium signals recorded via fiber
63 photometry was restricted to trials meeting the engagement criterion (Supp. Fig. 1F).
64 Importantly, this trial inclusion criteria allowed us to have a range of trials with different
65 reward zone and reward delivery latencies that did not significantly differ throughout

66 testing sessions (Supp. Fig. 1F) (See Methods). Moreover, it provided a suitable time
67 frame for investigating the activity of $PVT^{D2(+)}$ and $PVT^{D2(-)}$ neurons during different trial
68 groups and during different stages of the trials.

69 **$pPVT^{D2(+)}$ neuronal activity dynamics during food-seeking behavior**

70 We measured the activity of posterior $PVT^{D2(+)}$ ($pPVT^{D2(+)}$) neurons while food-restricted
71 mice performed trials in our foraging-like reward task. For this, we injected the PVT of
72 *Drd2*-Cre mice with an AAV driving expression of a Cre-dependent calcium sensor
73 (GCaMP6s) and recorded bulk fluorescence signals from this neuronal population using
74 fiber photometry (See Methods; Fig. 1A). At cue onset, we found no changes in the
75 averaged calcium signal in this population (Supp. Fig. 2A). However, we did find that
76 $pPVT^{D2(+)}$ neurons were robustly activated as mice approached the reward zone and the
77 receptacle to obtain the food reward (strawberry Ensure®; Fig. 1B). Modest but
78 statistically significant increases in calcium signals were also observed in these neuronal
79 populations upon reward delivery (Fig. 1C). Importantly, no such changes in fluorescence
80 were observed in control mice in which $pPVT^{D2(+)}$ neurons expressed GFP instead of
81 GCaMP (Fig. 1D-F). Collectively, these results demonstrate that $pPVT^{D2(+)}$ neurons are
82 modulated by reward-seeking and consumption.

83 To determine whether the activity of $pPVT^{D2(+)}$ neurons varied with the motivational state
84 of the subjects, we ranked all trials based on the latency to reach the reward zone (Fig.
85 1G) and divided them into five categories (L1–L5; Supp. Fig. 1G). Trials with the
86 shortest latencies to the reward zone (i.e., trials performed within 2- 3 sec; Fig. 1H)
87 were categorized as 'fast trials' (L1), whereas trials with the longest latencies (i.e., trials

88 performed within 9-11 sec; Fig. 1H) were categorized as 'slow trials' (L5). The trial
89 distribution for these two categories is shown in Supplemental Figure 1I, J. We next
90 compared the activity of pPVT$^{D2(+)}$ neurons during fast trials vs. slow trials. First our
91 analyses showed that the cue presentation calcium signal did not differ between fast or
92 slow approaches (Supp. Fig. 2B). However, during fast approach, pPVT$^{D2(+)}$ neurons
93 appeared to display higher GCaMP signal ramps compared to slow approach (Fig. 1I).
94 These differences in the GCaMP signal ramps were quantified by calculating the 20-
95 80% slope of the peak of GCaMP transients observed during the reward approach.
96 Quantifications of the signal's slope confirmed statistically significant differences in the
97 activity of pPVT$^{D2(+)}$ neurons between fast and slow trials (Fig. 1J). Moreover, we found
98 that both latency and velocity parameters were negatively correlated with the GCaMP
99 signals (Fig. 1K). Surprisingly, quantifications of the area under the curve (AUC) of the
100 signal (Fig.1L) revealed no significant differences between fast and slow trials.
101 Accordingly, no association was found between the latency to complete trials and signal
102 AUC or between the approach AUC and the approach slope (Fig. 1M). Lastly, no
103 changes in the activity of pPVT$^{D2(+)}$ neurons were observed when mice were moving
104 around the maze but were not engaged in the task (Fig. 1N). Altogether, our findings
105 thus far suggest that pPVT$^{D2(+)}$ neurons are modulated by reward-seeking and
106 consumption and that their activity varies with motivation.

107 To test if changes in need states impact pPVT$^{D2(+)}$ neuronal activity, we sorted trials by
108 trial order, categorizing the earliest trials as 'G1' and the latest trials as 'G5.' (Fig. 1O -
109 U). We implemented this strategy to model a satiety component, which assumes that
110 well-trained food-restricted mice are hungrier at the beginning compared to the end of

111 each 60 min testing session[21]. Importantly, the average latency to approach reward did
112 not show statistically significant differences across five trial groups distributed
113 throughout testing sessions (Supp. Fig. 1F; Fig.1Q). Previous research has shown that
114 NAc-projecting neurons of the pPVT are engaged by hunger signals and changes in
115 glucose levels, suggesting that need states influence the activity of PVT neurons[11,13,22].
116 In agreement with this view, we found that the activity of $pPVT^{D2(+)}$ neurons was higher
117 during early compared to later trials, indicating that $pPVT^{D2(+)}$ neuronal activity is
118 modulated by the satiety levels of subjects (Fig. 1R-T). Of note, quantifications of the
119 slope revealed no significant differences between early and late trials (Fig. 1U). We also
120 found that the activity of $pPVT^{D2(+)}$ neurons at reward delivery (Fig. 1V) and during cue
121 presentation (Supp. Fig 2C) trended towards a reduction as the session progressed, but
122 these changes were not statistically significant. Importantly, the observed decreases in
123 the activity of $pPVT^{D2(+)}$ neurons were unlikely due to photobleaching of the GCaMP
124 signal, as no statistically significant decreases in fluorescence signal were observed in
125 GFP controls (Fig.1W). To probe our conclusions further, GCaMP-expressing mice in
126 $pPVT^{D2(+)}$ neurons were tested in a separate session where the reward was completely
127 omitted for all trials. We observed that, under these conditions, these neurons were
128 highly active across trials (Supp. Fig. 2D, E), and unlike for rewarded trials, this activity
129 did not vary throughout sessions (Supp. Fig. 2F,G). Notably, 'fast trials' still displayed
130 significantly higher GCaMP ramps compared to 'slow trials', again supporting the notion
131 that the activity dynamics of $pPVT^{D2(+)}$ neurons reflect behavioral vigor (Supp. Fig. 2H,
132 I). Altogether, these findings suggest that $pPVT^{D2(+)}$ neuronal activity is influenced by

133 satiety levels, with higher activity observed early on in test sessions and lower activity
134 observed towards the end of sessions as satiety levels increase.

135 **Functional linear mixed model analysis of trial-level temporal dynamics for**
136 **pPVT$^{D2(+)}$ neuronal activity.**

137 Up to this point, we performed analyses of photometric signals for pPVT$^{D2(+)}$ neurons
138 based on either latency or trial order. However, these analyses involved condensing trial
139 types into summary measures, which obscures trial-level information. To mitigate this
140 limitation, we employed a new statistical framework for the analysis of fiber photometry
141 signals based on functional linear mixed modeling (FLMM)[23,24] to further explore the
142 relationship between the temporal structure of photometric signals and task-related
143 covariates. FLMM combines mixed-effects modeling and functional regression to account
144 for nested experimental studies containing multiple events in a trial and autocorrelations
145 in the photometry signal (see Methods). The result of this analysis is a single plot of the
146 coefficient estimates for each covariate (e.g., approach latency), which shows the
147 timepoints at which covariates have a statistically significant association with the
148 photometry signal across trials. Using FLMM, we then tested the effects of latency and
149 trial order during the following approach-related events: 1. cue presentation; and 2.
150 reward zone arrival (Supp. Fig. 3). For pPVT$^{D2(+)}$ neurons, FLMM showed an effect of
151 trial order but not latency on the magnitude of the photometry signal (Supp. Fig. 3A, B).
152 The lack of latency effect on signal is surprising considering that GCaMP signal in
153 pPVT$^{D2(+)}$ neurons rose more rapidly for fast compared to slow trials (Fig. 1J). One
154 potential reason for this discrepancy is that FLMM was performed on relatively short time
155 series surrounding discrete events. As such, when aligning signal to cue onset and

156 reward zone arrival, a significant fraction of approach-related signal dynamic might have
157 been missed. Of note, FLMM analysis generally yielded more nuanced information of how
158 photometry signal collected from pPVT$^{D2(+)}$ relates to behavior. Specifically, we found a
159 trial order effect on pPVT$^{D2(+)}$ neuronal activity during cue presentation and during reward
160 zone entry. These effects revealed a negative relationship between trial order and
161 photometry signal, such that as the mice performed more trials in a session, the pPVT^{D2+}
162 neuronal signal significantly decreased during cue presentation and around reward zone
163 entry (Supp Fig. 3B). Altogether, FLMM offers a robust statistical framework that can
164 extract meaningful information about the temporal structure of calcium traces across trials
165 and subjects in a task. As such, for the remainder of our study, we contrast our
166 observations based on summary measures with those yielded by FLMM.

167 **PVT$^{D2(-)}$ neuronal activity dynamics during food-seeking behavior**

168 We next examined the PVT$^{D2(-)}$ neuronal population and asked whether their activity
169 dynamics during the reward foraging task differ from that of PVT$^{D2(+)}$ neurons. For this,
170 the pPVT of *Drd2*-Cre mice was injected with an AAV driving expression of GCaMP6s
171 exclusively in Cre negative neurons (CreOFF; pPVT$^{D2(-)}$) and fiber photometry was used
172 to measure their activity in well-trained mice performing the reward task (Fig. 2A). We
173 found that, unlike pPVT$^{D2(+)}$ neurons, the activity of pPVT$^{D2(-)}$ neurons significantly
174 decreased during both reward approach and reward delivery (Fig. 2B, C). Given that,
175 like pPVT$^{D2(+)}$ neurons, the activity of pPVT$^{D2(-)}$ neurons is modulated during reward
176 approach and delivery, we then sought to assess whether the activity of pPVT$^{D2(-)}$
177 neurons could also be influenced by motivational factors. For this, we grouped trials
178 based on their latency to reach the reward zone as described earlier (Fig. 2D, E; Supp.

179 Fig. 1H, K, L). Interestingly, the slope of downward ramps did not significantly differ
180 between the two trial types (Fig. 2F, G), nor was there any correlation between the
181 slope and the latency to reward approach or trial velocity (Fig. 2H, I). There was no
182 statistically significant effect on AUC for fast and slow trials (Fig. 2J). These findings
183 indicate that pPVT$^{D2(-)}$ neuronal activity decreases during the reward approach, but
184 these decreases might not be associated with motivation-related parameters such as
185 latency to complete trials. Next, to investigate whether need states impact the activity of
186 pPVT$^{D2(-)}$ neurons, we categorized trials by trial order as noted earlier (Fig. 2K, L). Our
187 analyses revealed that unlike for pPVT$^{D2(+)}$ neurons, GCaMP signal recorded from
188 pPVT$^{D2(-)}$ neurons displayed no statistically significant difference between early (G1) and
189 late (G5) trials (Fig. 2L). These findings suggest that reward approach-related
190 population dynamics in pPVT$^{D2(-)}$ neurons might not be sensitive to hunger states. To
191 further assess our conclusions drawn from summary statistics, we again used FLMM to
192 test the effects of latency and trial order on trial level responses (Supp. Fig. 3). In
193 agreement with our earlier conclusions, FLMM revealed no association between either
194 satiety nor vigor-related metrics and signal dynamics in pPVT$^{D2(-)}$ neurons (Supp. Fig.
195 3C, D).

196 Previous studies have also suggested that the anterior PVT (aPVT), where PVT$^{D2(-)}$
197 neurons are most abundant[15,16], modulates food-seeking and feeding behavior and is
198 innervated by hypothalamic neurons that signal satiety[6,25,26]. Therefore, in a subset of
199 mice, we recorded aPVT$^{D2(-)}$ neurons while animals performed in our foraging-like
200 reward task (Fig, 2M). Our findings showed that, like pPVT$^{D2(-)}$ neurons, GCaMP
201 fluorescence in aPVT$^{D2(-)}$ neurons significantly decrease during reward approach and

202 reward zone entry (Fig. 2N, O), suggesting that $PVT^{D2(-)}$ neurons are functionally similar
203 irrespective of their antero-posterior location in the PVT. Moreover, grouping trials
204 based on either latency and trial order revealed no associations between these
205 parameters and signal (Fig. 2P-W), a conclusion that was further supported by FLMM
206 analysis (Supp. Fig. 3E, F). It is important to note that our independent assessment of
207 the activity dynamics of $pPVT^{D2(-)}$ and $aPVT^{D2(-)}$ neurons assumes that these two belong
208 to a largely homogenous subpopulation of PVT neurons. To directly test this prediction,
209 we used FLMM and included recording location (i.e., aPVT or pPVT) as a covariate in
210 our model. These analyses revealed no major effect of recording location cue and
211 reward zone-related signal dynamics (Supp. Fig. 3G), thus supporting the notion that
212 genetically-defined subpopulations of the PVT display similar functional properties
213 regardless of their location within the antero-posterior axis of the PVT[16].

214 **$PVT^{D2(+)}$ and $PVT^{D2(-)}$ neuronal activity dynamics during trial termination**

215 Previous studies, including those from our group, have established that PVT neuronal
216 activation is crucial for food-seeking behavior[11,13,22,27]. We now provide evidence that
217 $pPVT^{D2(+)}$ neurons are likely implicated in this process. However, other studies have
218 suggested that PVT neuron activation might also promote the suppression of reward-
219 seeking behavior[6,28,29]. This led us to hypothesize that $PVT^{D2(-)}$ neurons, albeit being
220 suppressed during the initiation of goal pursuits, signal the termination of such behaviors.
221 To test this prediction, we independently examined the *in vivo* dynamics of $pPVT^{D2(+)}$ and
222 $PVT^{D2(-)}$ neurons during 'trial termination,' defined as the moment when mice completed
223 reward consumption and began to return to the trigger zone to initiate another trial (Fig.
224 3A) (See Methods). Our analysis revealed that trial termination resulted in a reduction in

225 pPVT$^{D2(+)}$ neuronal activity (Fig. 3B) and significant increases in both pPVT$^{D2(-)}$ and
226 aPVT$^{D2(-)}$ neuronal activity (Fig. 3C, D), supporting our hypothesis that while pPVT$^{D2(+)}$
227 neurons signal reward approach, PVT$^{D2(-)}$ neurons signal the termination of food-seeking
228 behavior. Interestingly, when trials were sorted and binned by latency to return to the
229 trigger zone, neither pPVT$^{D2(+)}$, nor pPVT$^{D2(-)}$ neuronal activity was modulated by whether
230 mice performed a 'slow' or 'fast' return (Fig. 3E, F). Surprisingly, for aPVT$^{D2(-)}$, there was
231 not a main effect of return latency block, but pairwise comparisons between the slopes of
232 L1 and L5 revealed significant differences in aPVT$^{D2(-)}$ (Fig. 3G). These findings were
233 further supported by FLMM analysis which revealed a lack of effect of return latency on
234 pPVT$^{D2(+)}$ and pPVT$^{D2(-)}$ neuronal signaling for both trial termination and trigger zone entry
235 (Supp. Fig. 3H, J), and a main effect of return latency on aPVT$^{D2(-)}$ neuronal signal at both
236 termination and trigger zone entry (Supp. Fig. 3L). Lastly, when trials were sorted and
237 binned by trial order, we found no statistically significant modulation by the hunger state
238 of the animals for either neuronal type (Fig. 3H-J) and these findings were further
239 supported by FLMM (Supp. Fig. 3I, K, M). Altogether, our findings indicate that PVT$^{D2(-)}$
240 neuronal activity, but not pPVT$^{D2(+)}$, signals the termination of goal pursuits, and that
241 aPVT$^{D2(-)}$, but not pPVT$^{D2(-)}$ neuronal activity is influenced by motivation-related metrics
242 such as latency to return to the trigger zone after trial termination.

243 **pPVT$^{D2(+)}$–NAc and aPVT$^{D2(-)}$–NAc terminals display similar activity dynamics to**
244 **pPVT$^{D2(+)}$ and PVT$^{D2(-)}$ neurons.**

245 Approximately 80% of PVT neurons project to the NAc[30], including both PVT$^{D2(+)}$ and
246 PVT$^{D2(-)}$ neuronal subtypes[4,16,31]. Of note, the NAc plays a critical role in the learning
247 and execution of goal-oriented behaviors[18,32-34]. For this reason, we next investigated

248 how calcium signals recorded from the terminals of $PVT^{D2(+)}$ and $PVT^{D2(-)}$ neurons over
249 the NAc correlate with task and behavior variables in our reward foraging-like behavioral
250 task (Fig. 4). First, we used the same clustering analyses described earlier to compare
251 the activity dynamics of these terminals between trials with different latencies and those
252 at different stages of the session (Supp. Fig. 1H). Our results demonstrate that
253 $pPVT^{D2(+)}$–NAc terminals mirror the activity dynamics of $pPVT^{D2(+)}$ neurons (Fig. 4A - L).
254 Specifically, we observed robust increases in the fluorescence of $pPVT^{D2(+)}$–NAc
255 terminals during the reward approach, followed by a bi-phasic response at reward
256 delivery (Fig. 4A - C). In addition, $pPVT^{D2(+)}$–NAc terminals showed higher GCaMP
257 signal ramps during fast trials compared to slow trials (Fig. 4D - F). We also found a
258 negative correlation between approach latency and the slope of GCaMP signals, as well
259 as a positive correlation between velocity to approach the reward and the slope of the
260 GCaMP signal (Fig. 4G, H). This relationship between latency and signal was
261 corroborated by FLMM (Supp. Fig. 3O). Surprisingly, and unlike for $pPVT^{D2(+)}$ cell
262 bodies, by assessing average signals across trial order groups we did not observe a
263 statistically significant difference in the GCaMP signal of $pPVT^{D2(+)}$–NAc terminals
264 between early and late trials (Fig. 4J - K). However, FLMM analysis of $pPVT^{D2(+)}$–NAc
265 terminal recordings revealed a trial order effect at approximately 1s following reward
266 zone entry (Supp. Fig. 3P). This discrepancy between our summary statistics analysis
267 and FLMM, likely results from the capacity of the latter to assess significant associations
268 at any given timepoint during each trial[23]. We also found that $pPVT^{D2(+)}$–NAc terminals
269 showed a significant decrease in activity during trial termination (Fig. 4L) and FLMM
270 analysis revealed both latency and trial order effects after trial termination and trigger

271 zone entry (Supp. Fig. 3S, T). Collectively, these results suggest that decreases in
272 pPVT$^{D2(+)}$–NAc terminal activity are associated with trial termination and/or task
273 disengagement, and that termination-associated responses are modulated by both
274 motivation and satiety.
275 Finally, analysis of aPVT$^{D2(-)}$–NAc terminal activity demonstrated similar dynamics to the
276 broader aPVT$^{D2(-)}$ neuronal population (Fig. 4M – X). Specifically, aPVT$^{D2(-)}$–NAc
277 terminals displayed significant decreases in activity during the reward approach and
278 delivery (Fig. 4N, O). However, analysis of average signals for each trial type showed
279 no significant differences in the activity of aPVT$^{D2(-)}$–NAc terminals between fast vs.
280 slow approach or early vs. late trials (Fig.4P -W). Lastly, trial termination resulted in
281 increases in the activity of aPVT$^{D2(-)}$–NAc terminals (Fig. 4X). To gain further insight into
282 the association of parameters such as latency and trial order on the approach and
283 termination dynamics of aPVT$^{D2(-)}$–NAc terminal we used FLMM. Like for aPVT$^{D2(-)}$
284 neurons, FLMM showed no effect of trial order on signal magnitude during reward
285 approach (Supp. Fig. 3R). However, an effect of latency on signal was observed ahead
286 of reward zone entry (Supp. Fig. 3Q). FLMM also revealed an association between
287 latency to return to the trigger zone, but not trial order, and signal for aPVT$^{D2(-)}$–NAc
288 terminals (Supp. Fig. 3U, V), suggesting that like aPVT$^{D2(-)}$ cell bodies, these terminals
289 are sensitive to motivation-related variables. Collectively, our findings strongly suggest
290 that motivation-related features and the encoding of goal-oriented actions of pPVT$^{D2(+)}$
291 and PVT$^{D2(-)}$ neurons are being relayed to the NAc through their respective terminals.
292
293 **DISCUSSION**

294 We have identified two parallel thalamo-striatal pathways, namely $PVT^{D2(+)}$–NAc and
295 $PVT^{D2(-)}$–NAc, whose *in vivo* dynamics respectively encode the initiation and termination
296 of goal pursuits. In addition, we found that activity in these pathways, particularly the
297 $PVT^{D2(+)}$–NAc, mirrors that of the broader $PVT^{D2(+)}$ and $PVT^{D2(-)}$ neuronal populations and
298 tracks the motivational state of subjects. These results are consistent with the notion that
299 the PVT–NAc pathway guides motivated behaviors and offer a framework for interpreting
300 seemingly contradictory findings from the literature, where manipulations of the PVT
301 either increase or decrease reward seeking[6,10,11,13,16,22,25-29,35-38]. Indeed, our studies
302 support the notion that the dorsal midline thalamus integrates signals about need states
303 to shape goal-oriented behaviors[8,12,14,27,39]. Below, we discuss in detail our major findings
304 and frame them within the broader context of the literature.

305 The PVT has rapidly emerged as an important node guiding motivated behaviors, a
306 process that is thought to be mediated by its ability to integrate interoceptive signal and
307 cognitive information to guide goal-oriented actions[8,12,14,27,39]. For instance, recent
308 research has proposed that the activity of PVT neurons is modulated by hypothalamic-
309 derived neuromodulators such as orexin and neuropeptide Y to promote need states and
310 drive approach behaviors[13,40]. The PVT's role in guiding both appetitive and aversive-
311 motivated goal-oriented actions is thought to be largely dependent on its projections to
312 the NAc[1,4,5,10,11,37,41]. Of note, some studies have suggested that state-dependent
313 increases in PVT–NAc signaling are directly proportional to increased goal seeking
314 behavior[1,5,11,13,22]. For example, studies investigating single-cell PVT–NAc activity have
315 shown that putative inhibitory hypothalamic projections to the PVT are relaying licking
316 information[10]. These inhibitory hypothalamic inputs could be sending information to the

317 PVT regarding the hunger state of the animals. In line with these, NAc projecting PVT
318 neurons have also been shown to develop cues responses which have been shown to
319 depend on the animal's hunger state and hypothalamic derived signals such as
320 orexin[10,13,40]. These findings support the notion that need-based signals are conveyed to
321 the PVT to regulate motivated behaviors in response to changes in internal states. On the
322 other hand, others have argued that this relationship is rather inverse, for example, recent
323 studies have shown that aPVT neurons[6,25] and a subset of pPVT neurons[28,42] mediate
324 inappropriate reward-seeking behavior. Also, optogenetic activation of such PVT neurons
325 inhibited active lever pressing in a sucrose-seeking task[6,28,29,42]. Here, we propose that
326 thalamo-striatal projections arising from molecularly distinct subpopulations of the PVT
327 are responsible for such seemingly contradictory observations. Specifically, we suggest
328 that the striatal projections of $PVT^{D2(+)}$ and $PVT^{D2(-)}$ neurons, respectively, promote the
329 initiation and termination of goal pursuits (but see [42]). Our model appears in line with the
330 differential anatomical distribution of PVT projections to the NAc[30], and the known
331 differential contribution of NAc subregions to goal-oriented behaviors[32,33,43,44]. In a recent
332 publication, it was shown that while $PVT^{D2(+)}$ neurons predominantly innervate the core
333 and ventromedial shell of the NAc, the projections of $PVT^{D2(-)}$ neurons largely concentrate
334 in the dorsomedial shell and appear to be absent from the core[16]. Indeed, in the present
335 study, we aimed to target the medial shell, a region where the two subtypes overlap in
336 the NAc. However, future studies should aim to investigate whether the anatomical
337 dissociation of $PVT^{D2(+)}$ and $PVT^{D2(-)}$ afferents to the NAc underlies their differential
338 involvement in shaping instrumental actions.

339 It is worth noting that functional studies using patch-clamp electrophysiology have also
340 identified differential connectivity between the PVT and specific neuronal subclasses of
341 the NAc. Indeed, PVT axons have been shown to innervate NAc D1 medium spiny
342 neurons (MSNs), D2 MSNs, cholinergic interneurons, and parvalbumin
343 interneurons[1,28,42,45-48], and some studies have argued that the PVT's connectivity with
344 specific NAc subclasses is selective and/or modulated in an experience and/or-
345 dependent manner[1,28,42,47,48]. Future studies should investigate whether selective
346 connectivity between the PVT and specific NAc subtypes maps onto either $PVT^{D2(+)}$ or
347 $PVT^{D2(-)}$-derive input, and how this differential connectivity influences diverse aspects of
348 motivated behaviors.

349 One critical aspect of our study is that, in addition to assessing photometry responses
350 using standard approaches that rely on summary statistics, we have used a novel
351 statistical framework, termed FLMM[23], which enables hypothesis testing at every trial
352 time point and focuses on trial-level signals (no averaging). Of note, while FLMM helped
353 validate some of our conclusions drawn from summary statistics, it also yielded more
354 nuanced information particularly regarding the magnitude and temporal distribution of
355 effects. For example, FLMM uncovered an inverse relationship between trial order and
356 signal magnitude at cue onset for $pPVT^{D2(+)}$ neurons that was initially missed when
357 averaged responses across groups were assessed. In addition, FLMM enabled
358 statistical comparisons of responses drawn from $PVT^{D2(-)}$ neurons within different PVT
359 subregions, suggesting that responses in this population are rather similar and largely
360 independent of anatomical location. Thus, our findings support the notion that FLMM is

361 a robust statistical framework that facilitates extracting meaningful observations from
362 fiber photometry signals[23].

363 Here, we have shown that pPVT$^{D2(+)}$ neurons and their projections to the NAc display
364 similar response profiles and mirror motivational variables such as behavioral vigor and
365 sensitivity to satiety levels. This observation is consistent with prior studies showing that
366 PVT neuronal responses to motivational cues are shaped by state dependent
367 processes, as highlighted earlier[6,13]. It is worth noting that while the responses of
368 PVT$^{D2(-)}$ neurons were similarly consistent across anatomical location (aPVT vs pPVT)
369 and striatal projections (aPVT$^{D2(-)}$–NAc), some key differences were observed.
370 Specifically, unlike pPVT$^{D2(-)}$ neurons, both aPVT$^{D2(-)}$ neurons and their projections to the
371 NAc appeared to be sensitive to motivation-related metrics such as latency to initiate
372 and terminate a goal-oriented action and level of satiety. Although it is possible that
373 these differences reflect a unique capacity of the aPVT$^{D2(-)}$ population to track state-
374 dependent information, an alternative interpretation is that these discrepancies arise
375 from the differences in the sample sizes included in our analyses. Indeed, our pPVT$^{D2(-)}$
376 dataset includes one third fewer trials than both our aPVT$^{D2(-)}$ and aPVT$^{D2(-)}$–NAc
377 datasets. Future studies should investigate whether these potential differences across
378 PVT$^{D2(-)}$ populations are biologically relevant.

379 It is intriguing that while serving complementary functions in the initiation and
380 termination of goal-oriented behaviors, the activity of PVT$^{D2(+)}$ and PVT$^{D2(-)}$ neurons
381 appears to be largely mutually exclusive, with PVT$^{D2(+)}$ neurons activated at initiation
382 when PVT$^{D2(-)}$ activity is suppressed and PVT$^{D2(-)}$ neurons becoming activated at
383 termination when PVT$^{D2(+)}$ activity is reduced. Similar opposing dynamics were

384 observed in PVT subpopulations while mice engaged in mutually exclusive defensive
385 responses[5]. While this pattern of activity suggests that an inhibitory relationship exists
386 between these two neuronal classes, the rodent thalamus (including PVT) is largely
387 devoid of interneurons[49,50], and $PVT^{D2(+)}$ and $PVT^{D2(-)}$ neurons are not synaptically
388 connected to one another[16]. One potential mechanism for mediating the inhibitory
389 interaction between these two functional subclasses of the PVT is the thalamic reticular
390 nucleus (TRN). The TRN is a thin sheet of GABAergic neurons that surrounds the
391 thalamus and is known to play a key role in gating sensory information by modulating
392 thalamo-cortical transmission[50,51]. Recent work confirms earlier anatomical models
393 suggesting that the TRN mediates interactions between different thalamic nuclei[51-54].
394 Although largely speculative at present, in the context of the PVT, it is possible that the
395 TRN plays a similar role in mediating interactions between the $PVT^{D2(+)}$ and $PVT^{D2(-)}$
396 pathways. Specifically, the TRN may act as a hub that receives input from both
397 pathways and modulates their respective activities through inhibitory interactions,
398 resembling an open-loop configuration[55,56]. Of note, recent experimental evidence
399 supports the notion that an open-loop configuration involving PVT and TRN likely
400 exists[57]. Such architecture could allow for fine-tuning of goal-oriented behavior (i.e.,
401 engagement and disengagement of actions) by ensuring that the appropriate PVT–NAc
402 pathway is activated or inhibited at any given time. Future work should be aimed at
403 empirically testing this prediction.

404 Although here we have shown that two major subtypes of PVT neurons, namely
405 $PVT^{D2(+)}$ and $PVT^{D2(-)}$, differentially signal the initiation and termination of reward-
406 seeking, likely through their projections to the NAc, our classification might have limited

407 our ability to extract more nuanced information of how PVT subpopulations contribute to
408 goal-oriented behaviors. Indeed, recent research using single-cell RNA sequencing has
409 identified at least five potential molecularly distinct PVT subtypes[15] (See also[19]).
410 Importantly, the study concluded that a major node of separation across
411 transcriptomically distinct PVT neurons lies in the expression of dopamine D2 receptor
412 gene *Drd2*, such that $PVT^{D2(+)}$ neurons can be further subdivided into two subtypes:
413 *Esr1*$^{+}$ and *Col12a1*$^{+}$, while $PVT^{D2(-)}$ can be separated into two additional subtypes:
414 *Npffr1*$^{+}$ and *Hcrtr1*$^{+}$. A fifth subpopulation of PVT neurons is distributed across the
415 antero-posterior axis of the PVT and expresses *Drd3*[15]. Of note, according to Gao et al.,
416 2023, the five major PVT subclasses also display marked heterogeneity. Thus, while
417 our findings provide valuable insights into the role of PVT subtypes in motivated
418 behaviors, future studies should investigate the contributions of other PVT
419 subpopulations to fully understand the complex dynamics of the PVT–NAc circuitry. For
420 instance, it is possible that some of the functional differences in $PVT^{D2(-)}$ neurons
421 observed across the antero-posterior axis of the PVT map onto discrete subpopulations
422 of *Drd2*-negative neurons.

423 Some additional limitations of our study deserve to be acknowledged. Here, we have
424 monitored the activity of $PVT^{D2(+)}$ and $PVT^{D2(-)}$ neurons and how they relate to the
425 performance of motivated behavior in mice. As such, we cannot conclude that the
426 activity dynamics we have uncovered are causally related to the different aspects of
427 goal-oriented behavior that they appear to correlate with. Moreover, due to the nature of
428 the fiber photometry technique, it is possible that the observed responses in PVT
429 neuronal activity we report here represent the combined responses of additional PVT

430 subpopulations beyond $PVT^{D2(+)}$ and $PVT^{D2(-)}$ neurons. Indeed, while five molecularly
431 distinct PVT cells were recently described, top markers within these subpopulations
432 displayed minimal overlap with one another suggesting that additional cell-type
433 heterogeneity likely exists within the PVT. Another important limitation is that our
434 experiments were conducted exclusively during the light (inactive) phase. Considering
435 that previous studies have demonstrated diurnal variability in the intrinsic activity and
436 membrane properties of PVT neurons[58], it would be important to investigate how time of
437 day impacts the activity dynamics of $PVT^{D2(+)}$ and $PVT^{D2(-)}$ neurons described in our
438 study. Finally, it is crucial to acknowledge that our study has demonstrated consistent
439 responses among $PVT^{D2(-)}$ neurons in our task, regardless of their antero-posterior
440 location. However, it is important to note that our focus was exclusively on tracking the
441 activity of $PVT^{D2(+)}$ neurons in the pPVT. This decision stemmed from the sparse
442 distribution of $PVT^{D2(+)}$ neurons in the most anterior segments of the aPVT, as
443 documented by Gao et al. (2020). While this approach was chosen for practical
444 reasons, it is essential to highlight the absence of comparisons across the various
445 antero-posterior locations of the PVT for this neuronal population.

446 The findings presented here shed light on the neural circuits that underlie motivated
447 behaviors, including initiation, vigor, and termination. These processes are central to
448 achieving goals and maintaining appropriate levels of motivation in everyday life.
449 However, deficits in motivation are associated with a range of psychiatric conditions,
450 such as substance abuse, binge eating, and anhedonia in depression[59,60]. Therefore, a
451 deeper understanding of the neural basis of motivated behavior may offer new insights
452 into the treatment of these debilitating conditions. By revealing the specific neuronal

453 pathways involved in motivation and how they interact, this research may facilitate the
454 identification of new therapeutic targets for interventions aimed at restoring healthy
455 motivational processes in individuals with such conditions.
456

457 **ACKNOWLEDGEMENTS**

458 We thank Dr. Kirstie Cummings, Dr. Jeremy Day, Dr. Ryan Lingg and Briana Machen for
459 their comments on the manuscript. We also thank the NIHM Section on Instrumentation
460 for their contribution to building the foraging maze apparatus, the NIMH Rodent Behavior
461 Core for their assistance in the behavioral experiments, and the NIMH Systems
462 Neuroscience Imaging Resource. This work was supported by K99/R00 MH126429 to
463 S.B., a NARSAD Young Investigator Award by the Brain and Behavior Research
464 Foundation to S.B., and by the NIMH Intramural Research Program (1ZIAMH002950) to
465 M.A.P.
466

467 **AUTHOR CONTRIBUTIONS**

468 S.B. performed and analyzed all experiments. I.K., A.B., and S.R.G. assisted with
469 behavioral experiments. C.G. assisted with surgical techniques. G.L. and F.P. assisted
470 with the FLMM analyses. I.K. and E. M. assisted with data analysis. I.K. assisted with
471 histology procedures. S.B. and M.A.P. designed the study and interpreted the results.
472 S.B. and M.A.P. wrote the paper.
473

474 **COMPETING INTERESTS**

475 The authors declare no competing interests.

REFERENCES

1. Zhu, Y., Wienecke, C.F., Nachtrab, G., and Chen, X. (2016). A thalamic input to the nucleus accumbens mediates opiate dependence. Nature *530*, 219-222. 10.1038/nature16954.
2. Parsons, M.P., Li, S., and Kirouac, G.J. (2007). Functional and anatomical connection between the paraventricular nucleus of the thalamus and dopamine fibers of the nucleus accumbens. J Comp Neurol *500*, 1050-1063. 10.1002/cne.21224.
3. Engelke, D.S., Zhang, X.O., O'Malley, J.J., Fernandez-Leon, J.A., Li, S., Kirouac, G.J., Beierlein, M., and Do-Monte, F.H. (2021). A hypothalamic-thalamostriatal circuit that controls approach-avoidance conflict in rats. Nat Commun *12*, 2517. 10.1038/s41467-021-22730-y.
4. Beas, B.S., Wright, B.J., Skirzewski, M., Leng, Y., Hyun, J.H., Koita, O., Ringelberg, N., Kwon, H.B., Buonanno, A., and Penzo, M.A. (2018). The locus coeruleus drives disinhibition in the midline thalamus via a dopaminergic mechanism. Nat Neurosci *21*, 963-973. 10.1038/s41593-018-0167-4.
5. Ma, J., du Hoffmann, J., Kindel, M., Beas, B.S., Chudasama, Y., and Penzo, M.A. (2021). Divergent projections of the paraventricular nucleus of the thalamus mediate the selection of passive and active defensive behaviors. Nat Neurosci *24*, 1429-1440. 10.1038/s41593-021-00912-7.
6. Do-Monte, F.H., Minier-Toribio, A., Quinones-Laracuente, K., Medina-Colon, E.M., and Quirk, G.J. (2017). Thalamic Regulation of Sucrose Seeking during Unexpected Reward Omission. Neuron *94*, 388-400 e384. 10.1016/j.neuron.2017.03.036.
7. Campus, P., Covelo, I.R., Kim, Y., Parsegian, A., Kuhn, B.N., Lopez, S.A., Neumaier, J.F., Ferguson, S.M., Solberg Woods, L.C., Sarter, M., and Flagel, S.B. (2019). The paraventricular thalamus is a critical mediator of top-down control of cue-motivated behavior in rats. Elife *8*. 10.7554/eLife.49041.
8. McGinty, J.F., and Otis, J.M. (2020). Heterogeneity in the Paraventricular Thalamus: The Traffic Light of Motivated Behaviors. Front Behav Neurosci *14*, 590528. 10.3389/fnbeh.2020.590528.
9. Kirouac, G.J. (2015). Placing the paraventricular nucleus of the thalamus within the brain circuits that control behavior. Neurosci Biobehav Rev *56*, 315-329. 10.1016/j.neubiorev.2015.08.005.
10. Otis, J.M., Zhu, M., Namboodiri, V.M.K., Cook, C.A., Kosyk, O., Matan, A.M., Ying, R., Hashikawa, Y., Hashikawa, K., Trujillo-Pisanty, I., et al. (2019). Paraventricular Thalamus Projection Neurons Integrate Cortical and Hypothalamic Signals for Cue-Reward Processing. Neuron *103*, 423-431 e424. 10.1016/j.neuron.2019.05.018.
11. Beas, S., Gu, X., Leng, Y., Koita, O., Rodriguez-Gonzalez, S., Kindel, M., Matikainen-Ankney, B.A., Larsen, R.S., Kravitz, A.V., Hoon, M.A., and Penzo, M.A. (2020). A ventrolateral medulla-midline thalamic circuit for hypoglycemic feeding. Nat Commun *11*, 6218. 10.1038/s41467-020-19980-7.

12. Iglesias, A.G., and Flagel, S.B. (2021). The Paraventricular Thalamus as a Critical Node of Motivated Behavior via the Hypothalamic-Thalamic-Striatal Circuit. Front Integr Neurosci *15*, 706713. 10.3389/fnint.2021.706713.
13. Meffre, J., Sicre, M., Diarra, M., Marchessaux, F., Paleressompoulle, D., and Ambroggi, F. (2019). Orexin in the Posterior Paraventricular Thalamus Mediates Hunger-Related Signals in the Nucleus Accumbens Core. Curr Biol *29*, 3298-3306 e3294. 10.1016/j.cub.2019.07.069.
14. Kelley, A.E., Baldo, B.A., and Pratt, W.E. (2005). A proposed hypothalamic-thalamic-striatal axis for the integration of energy balance, arousal, and food reward. J Comp Neurol *493*, 72-85. 10.1002/cne.20769.
15. Gao, C., Gohel, C.A., Leng, Y., Ma, J., Goldman, D., Levine, A.J., and Penzo, M.A. (2023). Molecular and spatial profiling of the paraventricular nucleus of the thalamus. Elife *12*. 10.7554/eLife.81818.
16. Gao, C., Leng, Y., Ma, J., Rooke, V., Rodriguez-Gonzalez, S., Ramakrishnan, C., Deisseroth, K., and Penzo, M.A. (2020). Two genetically, anatomically and functionally distinct cell types segregate across anteroposterior axis of paraventricular thalamus. Nat Neurosci *23*, 217-228. 10.1038/s41593-019-0572-3.
17. Averbeck, B.B., and Costa, V.D. (2017). Motivational neural circuits underlying reinforcement learning. Nat Neurosci *20*, 505-512. 10.1038/nn.4506.
18. Kelley, A.E. (1999). Neural integrative activities of nucleus accumbens subregions in relation to learning and motivation. Psychobiology *27*, 198-213. 10.3758/BF03332114.
19. Shima, Y., Skibbe, H., Sasagawa, Y., Fujimori, N., Iwayama, Y., Isomura-Matoba, A., Yano, M., Ichikawa, T., Nikaido, I., Hattori, N., and Kato, T. (2023). Distinctiveness and continuity in transcriptome and connectivity in the anterior-posterior axis of the paraventricular nucleus of the thalamus. Cell Rep *42*, 113309. 10.1016/j.celrep.2023.113309.
20. Kvitsiani, D., Ranade, S., Hangya, B., Taniguchi, H., Huang, J.Z., and Kepecs, A. (2013). Distinct behavioural and network correlates of two interneuron types in prefrontal cortex. Nature *498*, 363-366. 10.1038/nature12176.
21. Jensen, T.L., Kiersgaard, M.K., Sorensen, D.B., and Mikkelsen, L.F. (2013). Fasting of mice: a review. Lab Anim *47*, 225-240. 10.1177/0023677213501659.
22. Labouebe, G., Boutrel, B., Tarussio, D., and Thorens, B. (2016). Glucose-responsive neurons of the paraventricular thalamus control sucrose-seeking behavior. Nat Neurosci *19*, 999-1002. 10.1038/nn.4331.
23. Loewinger, G., Cui, E., Lovinger, D., and Pereira, F. (2023). A Statistical Framework for Analysis of Trial-Level Temporal Dynamics in Fiber Photometry Experiments. bioRxiv. 10.1101/2023.11.06.565896.
24. Cui, E., Leroux, A., Smirnova, E., and Crainiceanu, C.M. (2022). Fast Univariate Inference for Longitudinal Functional Models. J Comput Graph Stat *31*, 219-230. 10.1080/10618600.2021.1950006.
25. Zhang, J., Chen, D., Sweeney, P., and Yang, Y. (2020). An excitatory ventromedial hypothalamus to paraventricular thalamus circuit that suppresses food intake. Nat Commun *11*, 6326. 10.1038/s41467-020-20093-4.
26. Cheng, J., Wang, J., Ma, X., Ullah, R., Shen, Y., and Zhou, Y.D. (2018). Anterior Paraventricular Thalamus to Nucleus Accumbens Projection Is Involved in

565 Feeding Behavior in a Novel Environment. Front Mol Neurosci *11*, 202.
566 10.3389/fnmol.2018.00202.
567 27. Millan, E.Z., Ong, Z., and McNally, G.P. (2017). Paraventricular thalamus:
568 Gateway to feeding, appetitive motivation, and drug addiction. Prog Brain Res
569 *235*, 113-137. 10.1016/bs.pbr.2017.07.006.
570 28. Vollmer, K.M., Green, L.M., Grant, R.I., Winston, K.T., Doncheck, E.M., Bowen,
571 C.W., Paniccia, J.E., Clarke, R.E., Tiller, A., Siegler, P.N., et al. (2022). An
572 opioid-gated thalamoaccumbal circuit for the suppression of reward seeking in
573 mice. Nat Commun *13*, 6865. 10.1038/s41467-022-34517-w.
574 29. Lafferty, C.K., Yang, A.K., Mendoza, J.A., and Britt, J.P. (2020). Nucleus
575 Accumbens Cell Type- and Input-Specific Suppression of Unproductive Reward
576 Seeking. Cell Rep *30*, 3729-3742 e3723. 10.1016/j.celrep.2020.02.095.
577 30. Dong, X., Li, S., and Kirouac, G.J. (2017). Collateralization of projections from
578 the paraventricular nucleus of the thalamus to the nucleus accumbens, bed nucleus
579 of the stria terminalis, and central nucleus of the amygdala. Brain Struct Funct *222*,
580 3927-3943. 10.1007/s00429-017-1445-8.
581 31. Clark, A.M., Leroy, F., Martyniuk, K.M., Feng, W., McManus, E., Bailey, M.R.,
582 Javitch, J.A., Balsam, P.D., and Kellendonk, C. (2017). Dopamine D2 Receptors in
583 the Paraventricular Thalamus Attenuate Cocaine Locomotor Sensitization. eNeuro
584 *4*. 10.1523/ENEURO.0227-17.2017.
585 32. Floresco, S.B. (2015). The nucleus accumbens: an interface between cognition,
586 emotion, and action. Annu Rev Psychol *66*, 25-52. 10.1146/annurev-psych-
587 010213-115159.
588 33. Floresco, S.B., McLaughlin, R.J., and Haluk, D.M. (2008). Opposing roles for the
589 nucleus accumbens core and shell in cue-induced reinstatement of food-seeking
590 behavior. Neuroscience *154*, 877-884. 10.1016/j.neuroscience.2008.04.004.
591 34. Ikemoto, S., and Panksepp, J. (1999). The role of nucleus accumbens dopamine in
592 motivated behavior: a unifying interpretation with special reference to reward-
593 seeking. Brain Res Brain Res Rev *31*, 6-41. 10.1016/s0165-0173(99)00023-5.
594 35. Zhang, X., and van den Pol, A.N. (2017). Rapid binge-like eating and body weight
595 gain driven by zona incerta GABA neuron activation. Science *356*, 853-859.
596 10.1126/science.aam7100.
597 36. Ong, Z.Y., Liu, J.J., Pang, Z.P., and Grill, H.J. (2017). Paraventricular Thalamic
598 Control of Food Intake and Reward: Role of Glucagon-Like Peptide-1 Receptor
599 Signaling. Neuropsychopharmacology *42*, 2387-2397. 10.1038/npp.2017.150.
600 37. Ye, Q., Nunez, J., and Zhang, X. (2022). Oxytocin Receptor-Expressing Neurons
601 in the Paraventricular Thalamus Regulate Feeding Motivation through Excitatory
602 Projections to the Nucleus Accumbens Core. J Neurosci *42*, 3949-3964.
603 10.1523/JNEUROSCI.2042-21.2022.
604 38. Betley, J.N., Cao, Z.F., Ritola, K.D., and Sternson, S.M. (2013). Parallel,
605 redundant circuit organization for homeostatic control of feeding behavior. Cell
606 *155*, 1337-1350. 10.1016/j.cell.2013.11.002.
607 39. Penzo, M.A., and Gao, C. (2021). The paraventricular nucleus of the thalamus: an
608 integrative node underlying homeostatic behavior. Trends Neurosci *44*, 538-549.
609 10.1016/j.tins.2021.03.001.

40. Horio, N., and Liberles, S.D. (2021). Hunger enhances food-odour attraction through a neuropeptide Y spotlight. Nature *592*, 262-266. 10.1038/s41586-021-03299-4.
41. Dong, X., Li, S., and Kirouac, G.J. (2020). A projection from the paraventricular nucleus of the thalamus to the shell of the nucleus accumbens contributes to footshock stress-induced social avoidance. Neurobiol Stress *13*, 100266. 10.1016/j.ynstr.2020.100266.
42. Paniccia, J.E., Vollmer, K.M., Green, L.M., Grant, R.I., Winston, K.T., Buchmaier, S., Westphal, A.M., Clarke, R.E., Doncheck, E.M., Bordieanu, B., et al. (2023). Restoration of a paraventricular thalamo-accumbal behavioral suppression circuit prevents reinstatement of heroin seeking. Neuron. 10.1016/j.neuron.2023.11.024.
43. Al-Hasani, R., McCall, J.G., Shin, G., Gomez, A.M., Schmitz, G.P., Bernardi, J.M., Pyo, C.O., Park, S.I., Marcinkiewcz, C.M., Crowley, N.A., et al. (2015). Distinct Subpopulations of Nucleus Accumbens Dynorphin Neurons Drive Aversion and Reward. Neuron *87*, 1063-1077. 10.1016/j.neuron.2015.08.019.
44. Chen, G., Lai, S., Bao, G., Ke, J., Meng, X., Lu, S., Wu, X., Xu, H., Wu, F., Xu, Y., et al. (2023). Distinct reward processing by subregions of the nucleus accumbens. Cell Rep *42*, 112069. 10.1016/j.celrep.2023.112069.
45. Lafferty, C.K., and Britt, J.P. (2020). Off-Target Influences of Arch-Mediated Axon Terminal Inhibition on Network Activity and Behavior. Front Neural Circuits *14*, 10. 10.3389/fncir.2020.00010.
46. Baimel, C., Jang, E., Scudder, S.L., Manoocheri, K., and Carter, A.G. (2022). Hippocampal-evoked inhibition of cholinergic interneurons in the nucleus accumbens. Cell Rep *40*, 111042. 10.1016/j.celrep.2022.111042.
47. Giannotti, G., Gong, S., Fayette, N., Heinsbroek, J.A., Orfila, J.E., Herson, P.S., Ford, C.P., and Peters, J. (2021). Extinction blunts paraventricular thalamic contributions to heroin relapse. Cell Rep *36*, 109605. 10.1016/j.celrep.2021.109605.
48. Joffe, M.E., and Grueter, B.A. (2016). Cocaine Experience Enhances Thalamo-Accumbens N-Methyl-D-Aspartate Receptor Function. Biol Psychiatry *80*, 671-681. 10.1016/j.biopsych.2016.04.002.
49. Arcelli, P., Frassoni, C., Regondi, M.C., De Biasi, S., and Spreafico, R. (1997). GABAergic neurons in mammalian thalamus: a marker of thalamic complexity? Brain Res Bull *42*, 27-37. 10.1016/s0361-9230(96)00107-4.
50. Halassa, M.M., and Acsady, L. (2016). Thalamic Inhibition: Diverse Sources, Diverse Scales. Trends Neurosci *39*, 680-693. 10.1016/j.tins.2016.08.001.
51. Halassa, M.M., Chen, Z., Wimmer, R.D., Brunetti, P.M., Zhao, S., Zikopoulos, B., Wang, F., Brown, E.N., and Wilson, M.A. (2014). State-dependent architecture of thalamic reticular subnetworks. Cell *158*, 808-821. 10.1016/j.cell.2014.06.025.
52. Wimmer, R.D., Schmitt, L.I., Davidson, T.J., Nakajima, M., Deisseroth, K., and Halassa, M.M. (2015). Thalamic control of sensory selection in divided attention. Nature *526*, 705-709. 10.1038/nature15398.
53. Zikopoulos, B., and Barbas, H. (2007). Circuits formultisensory integration and attentional modulation through the prefrontal cortex and the thalamic reticular nucleus in primates. Rev Neurosci *18*, 417-438. 10.1515/revneuro.2007.18.6.417.

54. Guillery, R.W., and Harting, J.K. (2003). Structure and connections of the thalamic reticular nucleus: Advancing views over half a century. J Comp Neurol *463*, 360-371. 10.1002/cne.10738.
55. Brown, J.W., Taheri, A., Kenyon, R.V., Berger-Wolf, T.Y., and Llano, D.A. (2020). Signal Propagation via Open-Loop Intrathalamic Architectures: A Computational Model. eNeuro *7*. 10.1523/ENEURO.0441-19.2020.
56. Willis, A.M., Slater, B.J., Gribkova, E.D., and Llano, D.A. (2015). Open-loop organization of thalamic reticular nucleus and dorsal thalamus: a computational model. J Neurophysiol *114*, 2353-2367. 10.1152/jn.00926.2014.
57. Quinones-Laracuente, K., Vega-Medina, A., and Quirk, G.J. (2021). Time-Dependent Recruitment of Prelimbic Prefrontal Circuits for Retrieval of Fear Memory. Front Behav Neurosci *15*, 665116. 10.3389/fnbeh.2021.665116.
58. Kolaj, M., Zhang, L., Ronnekleiv, O.K., and Renaud, L.P. (2012). Midline thalamic paraventricular nucleus neurons display diurnal variation in resting membrane potentials, conductances, and firing patterns in vitro. J Neurophysiol *107*, 1835-1844. 10.1152/jn.00974.2011.
59. Grahek, I., Shenhav, A., Musslick, S., Krebs, R.M., and Koster, E.H.W. (2019). Motivation and cognitive control in depression. Neurosci Biobehav Rev *102*, 371-381. 10.1016/j.neubiorev.2019.04.011.
60. Der-Avakian, A., Barnes, S.A., Markou, A., and Pizzagalli, D.A. (2016). Translational Assessment of Reward and Motivational Deficits in Psychiatric Disorders. Curr Top Behav Neurosci *28*, 231-262. 10.1007/7854_2015_5004.

680 **FIGURE LEGENDS**

681 **Figure 1. *In-vivo* activity dynamics of PVT$^{D2(+)}$ neurons.**

682 **(A)** *Left*: Schematic of the stereotaxic injections and optical fiber implantation for
683 targeting D2(+) neurons in the pPVT. *Right*: Representative image from a Drd2-Cre
684 mouse expressing GCaMP6s in the pPVT.

685 (**B)** *Left*: Average GCaMP6s responses from pPVT$^{D2(+)}$ neurons showing ramping
686 activity during reward approach. *Right*: Quantification of the approach-evoked changes
687 in GCaMP6s fluorescence in pPVT$^{D2(+)}$ neurons. Area under the curve (AUC), n = 296
688 trials from 6 mice, two-tailed paired t-test, ***$p<0.001$.

689 (**C)** *Left*: Average GCaMP6s responses from pPVT$^{D2(+)}$ neurons during reward delivery.
690 *Right*: AUC quantification of the reward-evoked changes in GCaMP6s fluorescence in
691 pPVT$^{D2(+)}$ neurons. n = 296 trials from 6 mice, two-tailed paired t-test, *$p<0.05$.

692 (**D)** *Left*: Top - Average GFP fluorescence during reward approach. Bottom - Average
693 GFP activity during reward delivery. *Middle:* AUC quantification of GFP fluorescence
694 during the baseline and approach periods. Two-tailed paired t-test, $p=0.29$; ns, not
695 significant. *Right:* AUC quantification of GFP fluorescence during the baseline and
696 reward delivery periods. Two-tailed paired t-test, $p=0.18$; ns, not significant.

697 (**E)** *Left*: AUC quantification between GFP and pPVT$^{D2(+)}$ neuronal activity during reward
698 approach. Two-tailed unpaired t-test, n = 544 trials from 5 mice, ***$p<0.001$. *Right:* AUC
699 quantification between GFP and pPVT$^{D2(+)}$ neuronal activity during reward delivery.
700 AUC, Two-tailed unpaired t-test, *$p<0.05$.

701 **(F)** Heatmap of GFP activity in the pPVT, time-locked to cue onset, sorted by trial order,
702 and binned into 5 'trial group blocks' (G1 – G5). Yellow dots represent reward zone
703 arrival.
704 (**G)** Heatmap showing excitatory reward approach responses from pPVT$^{D2(+)}$ neurons,
705 time-locked to cue onset, sorted by latency to approach the reward zone and binned
706 into 5 'approach latency blocks,' L1, n = 61 trials, L2, n= 67 trials, L3, n = 67 trials, L4, n
707 = 67 trials, L5, n = 64 trials from 6 mice.
708 **(H)** *Left*: Latencies to reach the reward zone in seconds for each approach latency
709 block. Repeated measures ANOVA, *****p<0.0001. Right*: Velocity (m/s) during reward
710 approach calculated for each approach latency block. Repeated measures ANOVA,
711 *****p<0.0001*.
712 **(I)** Average GCaMP6s responses for fast and slow reward approach. The red line
713 represents 20-80% of the slope of the line.
714 **(J)** Slope-of-the-line quantifications of GCaMP6s activity from pPVT$^{D2(+)}$ neurons across
715 approach latency blocks. Repeated measures ANOVA, ***p<0.01*.
716 **(K)** *Left:* Pairwise correlation between the approach latency and the slope-of-the-line
717 quantifications of GCaMP6s responses from pPVT$^{D2(+)}$ neurons during the approach.
718 *Right:* Correlation between the velocity (m/s) during the approach and the slope-of-the-
719 line quantifications of GCaMP6s responses from pPVT$^{D2(+)}$ neurons during the
720 approach. Each dot represents the GCaMP6s activity of individual mice averaged
721 across approach latency blocks.

722 **(L)** AUC quantifications of the reward approach-evoked changes in GCaMP6s activity
723 across approach latency blocks. Repeated measures ANOVA, *p=0.55;* ns, not
724 significant
725 **(M)***. Left:* No correlation between approach latency and AUC. *Right:* No correlation
726 between the AUC and the slope-of-the-line quantifications of GCaMP6s responses from
727 $pPVT^{D2(+)}$ neurons during the approach.
728 **(N)** Average GCaMP6s fluorescence from $pPVT^{D2(+)}$ neurons during spontaneous
729 locomotion.
730 **(O)** Same as (G), but responses were sorted by trial order and binned into 5 'trial group
731 blocks.' G1, n = 61 trials, G2, n= 67 trials, G3, n = 67 trials, G4, n = 67 trials, G5, n = 64
732 trials from 6 mice. Yellow dots represent reward zone arrival.
733 **(P)** Latencies to reach the reward zone across trial group blocks. Repeated measures
734 ANOVA, ***p<0.001*.
735 **(Q)** No correlation between the approach latency and trial order.
736 **(R)** Average GCaMP6s responses from $pPVT^{D2(+)}$ neurons comparing approach trials
737 performed early and late in the testing session. The red line indicates 20-80% of the
738 slope of the line.
739 **(S)** AUC quantification of the reward approach-evoked changes in GCaMP6s activity
740 across trial group blocks. Repeated measures ANOVA, ***p<0.001*.
741 **(T)** Correlation between the AUC of the reward approach-evoked changes in GCaMP6s
742 activity and trial order within a test session.
743 **(U)** Slope-of-the-line quantifications of GCaMP6s activity across trial group blocks.
744 Repeated measures ANOVA, *p=0.36*.

745 **(V)** *Left:* Average GCaMP6s responses from pPVT$^{D2(+)}$ neurons upon reward delivery
746 comparing early and late trials in the testing session. *Right:* AUC quantification during
747 reward delivery across trial group blocks. Repeated measures ANOVA, *p=0.36*; ns, not
748 significant.
749 **(W)** *Left:* Latencies to reach the reward zone across trial group blocks. Repeated
750 measures ANOVA, *p=0.25;* ns, not significant. *Middle:* Average GFP activity in the
751 pPVT comparing approach trials performed early or late in the testing session. *Right:*
752 AUC quantification of GFP activity in the pPVT during approach across trial group
753 blocks. Repeated measures ANOVA*, p=0.60*; ns, not significant.
754 All data in the figure are shown as mean ±s.e.m.

755

756 **Figure 2. *In-vivo* activity dynamics of pPVT$^{D2(-)}$ neurons.**

757 **(A)** *Left*: Schematic of the stereotaxic injections for selective expression of Cre-OFF
758 GCaMP6s viral vectors and fiber implantation to target D2(-) neurons in the pPVT.
759 *Right*: Representative image from a Drd2-Cre mouse expressing Cre-OFF GCaMP6s in
760 the pPVT.
761 **(B)** *Left*: Average GCaMP6s response from pPVT$^{D2(-)}$ neurons during reward approach.
762 *Right*: Quantification of the approach-evoked changes in GCaMP6s fluorescence in
763 pPVT$^{D2(-)}$ neurons. AUC, n = 420 trials from 6 mice, two-tailed paired t-test, **p<0.05*.
764 **(C)** *Left*: Average GCaMP6s responses from pPVT$^{D2(-)}$ neurons during reward delivery.
765 *Right*: AUC quantification of reward-evoked changes in GCaMP6s fluorescence in
766 pPVT$^{D2(-)}$ neurons. Two-tailed paired t-test, ***p<0.001*.

767 **(D)** Heatmap showing approach responses from pPVT$^{D2(-)}$ neurons, time-locked to cue
768 onset, sorted by latency to approach the reward zone, and binned into 5 'approach
769 latency blocks,' L1, n = 79 trials, L2, n= 81 trials, L3, n = 84 trials, L4, n = 87 trials, L5, n
770 = 89 trials from 6 mice.
771 **(E)** *Left*: Latencies to reach the reward zone for each latency block. Repeated measures
772 ANOVA ****$p<0.0001$. *Right*: Velocity (m/s) during reward approach calculated for each
773 latency block. Repeated measures ANOVA, ****$p<0.0001$.
774 **(F)** Average GCaMP6s dynamics for fast approach (L1) and slow approach (L5) in
775 pPVT$^{D2(-)}$ neurons. The red line indicates 20-80% of the slope of the line.
776 **(G)** Slope-of-the-line quantifications of GCaMP6s activity from pPVT$^{D2(-)}$ neurons across
777 approach latency blocks. Repeated measures ANOVA, $p=0.25$; ns, not significant.
778 **(H)** Correlation between the approach latency and the slope-of-the-line quantifications
779 of GCaMP6s responses during reward approach. Each dot represents the GCaMP6s
780 activity of individual mice averaged across approach latency blocks.
781 **(I)** Correlation between the velocity (m/s) during the approach and the slope-of-the-line
782 quantifications of GCaMP6s responses during the reward approach.
783 **(J)** AUC quantification of the reward approach-evoked changes in GCaMP6s activity
784 from pPVT$^{D2(-)}$ neurons across approach latency blocks. Repeated measures ANOVA,
785 $p=0.90$; ns, not significant.
786 **(K)** Same as (D), but responses were sorted by trial order and binned into 5 'trial group
787 blocks,' G1, n = 79 trials, G2, n= 81 trials, G3, n = 84 trials, G4, n = 87 trials, G5, n = 89
788 trials from 6 mice. Yellow dots represent reward zone arrival.

789 **(L)** *Left*: Latencies to reach the reward zone across trial group blocks. Repeated
790 measures ANOVA, *p=0.11;* ns, not significant. *Middle*: Average GCaMP6s responses
791 from pPVT$^{D2(-)}$ neurons comparing approach trials performed early and late in the testing
792 session. *Right*: AUC quantification of the reward approach-evoked changes in
793 GCaMP6s activity from pPVT$^{D2(-)}$ neurons across trial group blocks. Repeated measures
794 ANOVA, *p=0.93*; ns, not significant.
795 **(M)** *Left*: Schematic of stereotaxic injections and fiber implantation. *Right:* Representative
796 image of D2(-) neurons in the aPVT.
797 **(N)** *Left*: Average GCaMP6s response from aPVT$^{D2(-)}$ neurons showing decreases in
798 activity dynamics during reward approach. *Right:* AUC quantification of approach-evoked
799 changes in GCaMP6s fluorescence in aPVT$^{D2(-)}$ neurons. AUC, n = 650 trials from 8 mice,
800 two-tailed paired t-test, ****$p<0.0001$.
801 **(O)** *Left*: Average GCaMP6s response from aPVT$^{D2(-)}$ neurons showing decreased
802 activity dynamics during reward delivery. *Right:* AUC quantification of reward-evoked
803 changes in GCaMP6s fluorescence in aPVT$^{D2(-)}$ neurons. Two-tailed paired t-test,
804 *$p<0.05$.
805 **(P)** Heatmap showing approach responses of aPVT$^{D2(-)}$ neurons, time-locked to cue
806 onset, sorted by latency to approach the reward zone, and binned into 5 'approach
807 latency blocks' (L1 – L5), L1, n = 129 trials, L2, n= 129 trials, L3, n = 129 trials, L4, n =
808 129 trials, L5, n = 139 trials from 8 mice.
809 **(Q)** *Left*: Latencies to reach the reward zone in seconds (s) for each approach latency
810 block. Repeated measures ANOVA, ****$p<0.0001$. *Right:* Velocity (m/s) during reward

811 approach calculated for each approach latency block. Repeated measures ANOVA,

812 *****p<0.0001.*

813 **(R)** *Left*: Average GCaMP6s responses for fast and slow reward approach. The red line

814 indicates 20-80% of the slope of the line. *Right:* Slope-of-the-line quantifications of

815 GCaMP6s activity from aPVT$^{D2(-)}$ neurons across approach latency blocks. Repeated

816 measures ANOVA, *p=0.08*; ns, not significant

817 **(S)** Correlation between approach latency and the slope-of-the-line quantifications per

818 animal for each latency block.

819 **(T)** Correlation between approach velocity and the slope-of-the-line of the line

820 quantifications

821 **(U)** AUC quantification during reward approach across latency blocks. Repeated

822 measures ANOVA, **p<0.05;* L1 vs. L5 Tukey's multiple comparisons test, *p=0.14*.

823 **(V)** Same as (P), but responses were sorted by trial order and binned into 5 'trial group

824 blocks' (G1 – G5). Yellow dots represent reward zone arrival.

825 **(W)** *Left*: Quantification of latency of reward approach across trial group blocks. Repeated

826 measures ANOVA, **p<0.05;* G1 vs. G5 Tukey's multiple comparisons test, *p=0.99*.

827 *Middle:* Average GCaMP6s response for aPVT$^{D2(-)}$ neurons during trials performed early

828 (G1) and late (G5) during the session. *Right:* AUC quantification of GCaMP6s activity

829 during approach across trial group blocks. Repeated measures ANOVA, *p=0.29*; ns, not

830 significant.

831 All data in the figure are shown as mean ±s.e.m.

832

833 **Figure 3. PVT$^{D2(+)}$ and PVT$^{D2(-)}$ neurons *in vivo* dynamics during trial termination.**

834 **(A)** Schematic depicting animal return to the trigger zone in our foraging-like reward-
835 seeking task.
836 **(B)** *Left*: Average GCaMP6s responses from $pPVT^{D2(+)}$ neurons during trial termination
837 and return. *Right:* Quantification of the return-evoked changes in GCaMP6s
838 fluorescence in $pPVT^{D2(+)}$ neurons. AUC, two-tailed paired t-test, *$p<0.05$. *Bottom:* In a
839 complete trial, the activity dynamics of $pPVT^{D2(+)}$ neurons from a sample subject during
840 the reward foraging task are represented by the purple line, while the black ticks
841 indicate various events within the trial.
842 **(C)** *Left*: Average GCaMP6s responses from $pPVT^{D2(-)}$ neurons during trial termination
843 and return. *Right:* Quantification of the return-evoked changes in GCaMP6s
844 fluorescence in $pPVT^{D2(-)}$ neurons. AUC, two-tailed paired t-test, **$p<0.01$. *Bottom:*
845 Same as (B) for $pPVT^{D2(-)}$ neurons.
846 **(D)** *Left*: Average GCaMP6s responses from $aPVT^{D2(-)}$ neurons during trial termination
847 and return. *Right:* Quantification of the return-evoked changes in GCaMP6s
848 fluorescence in $aPVT^{D2(-)}$ neurons. AUC, two-tailed paired t-test, ***$p<0.001$.
849 **(E)** *Left:* Latencies to reach the trigger zone across approach latency blocks for
850 $pPVT^{D2(+)}$ neuronal imaging. Repeated measures ANOVA, ****$p<0.01$. *Middle:* Average
851 GCaMP6s dynamics for fast return (L1) and slow return (L5) in $pPVT^{D2(+)}$ neurons. The
852 red line indicates 20-80% of the slope of the line. *Right:* Slope-of-the-line quantification
853 of GCaMP6s return activity in $pPVT^{D2(+)}$ neurons. Repeated measures ANOVA, $p=0.45$;
854 ns, not significant.
855 **(F)** *Left:* Latencies to reach the trigger zone across approach latency blocks for $pPVT^{D2(-)}$
856 photometry recordings. Repeated measures ANOVA, ****$p<0.01$. *Middle:* Average

857 GCaMP6s dynamics for fast return (L1) and slow return (L5) in pPVT$^{D2(-)}$ neurons. The
858 red line indicates 20-80% of the slope of the line. *Right:* Slope-of-the-line quantification
859 of GCaMP6s return activity in pPVT$^{D2(-)}$ neurons across latency blocks. Repeated
860 measures ANOVA, *p=0.28*; ns, not significant.
861 **(G)** *Left:* Latencies to reach the trigger zone across approach latency blocks for aPVT$^{D2(-}$
862 $^{)}$ photometry recordings. Repeated measures ANOVA, ****$p<0.01$. *Middle:* Average
863 GCaMP6s dynamics for fast return (L1) and slow return (L5) in aPVT$^{D2(-)}$ neurons. The
864 red line indicates 20-80% of the slope of the line. *Right:* Slope-of-the-line quantification of
865 GCaMP6s return activity in aPVT$^{D2(-)}$ neurons across latency blocks. Repeated measures
866 ANOVA, *p=0.13;* G1 vs. G5 Tukey's multiple comparisons test.
867 **(H)** *Left:* Latencies to reach the trigger zone across trial group blocks for pPVT$^{D2(+)}$
868 photometry recordings. Repeated measures ANOVA, *p=0.29;* ns, not significant. *Middle:*
869 Average GCaMP6s return dynamics from pPVT$^{D2(+)}$ neurons comparing return trials
870 performed early and late in the testing session. *Right:* AUC quantification of GCaMP6s
871 activity during the return in pPVT$^{D2(+)}$ neurons across trial group blocks. Repeated
872 measures ANOVA, *p=0.71*; ns, not significant.
873 **(I)** *Left:* Latencies to reach the trigger zone across trial group blocks for pPVT$^{D2(-)}$
874 photometry recordings. Repeated measures ANOVA, *p=0.18;* ns, not significant. *Middle:*
875 Average GCaMP6s return dynamics in pPVT$^{D2(-)}$ neurons for early and late trials. *Right:*
876 AUC quantification of GCaMP6s activity during return in pPVT$^{D2(-)}$ neurons across trial
877 group blocks. Repeated measures ANOVA, *p=0.76*; ns, not significant.
878 **(J)** *Left:* Latencies to reach the trigger zone across trial group blocks for aPVT$^{D2(-)}$
879 photometry recordings. Repeated measures ANOVA, *$p<0.05$; G1 vs. G5 Tukey's

880 multiple comparisons test, *p=0.16*. *Middle:* Average GCaMP6s return dynamics in
881 aPVT$^{D2(-)}$ neurons for early and late trials. *Right:* AUC quantification of GCaMP6s activity
882 during return in aPVT$^{D2(-)}$ neurons across trial group blocks. Repeated measures
883 ANOVA, *p=0.54*; ns, not significant.
884 All data in the figure are shown as mean ±s.e.m.
885
886 **Figure 4. *In vivo* activity dynamics of PVT$^{D2(+)}$–NAc and PVT$^{D2(-)}$–NAc axon**
887 **terminals.**
888 **(A)** *Left*: Schematic of stereotaxic injections and fiber implantation. *Right:*
889 Representative images of GCaMP6s expression in D2(+) neurons in the pPVT and fiber
890 placement in NAc.
891 **(B)** *Left*: Average GCaMP6s approach-evoked responses from pPVT$^{D2(+)}$ terminals
892 during the reward approach. *Right*: Quantification of the approach-evoked changes in
893 GCaMP6s fluorescence in pPVT$^{D2(+)}$ terminals. AUC, n = 330 trials from 4 mice, two-
894 tailed paired t-test, *$p<0.05$.
895 **(C)** *Left*: GCaMP6s reward-evoked response in pPVT$^{D2(+)}$ terminals during reward
896 delivery. *Right*: Quantification of the reward-evoked changes in GCaMP6s fluorescence
897 in pPVT$^{D2(+)}$ terminals. AUC, two-tailed paired, *p=0.08*; ns, not significant.
898 **(D)** Heatmap showing excitatory reward approach responses of pPVT$^{D2(+)}$ terminals,
899 time-locked to cue onset, sorted by latency to approach the reward zone, and binned
900 into 5 'approach latency blocks' (L1 – L5). L1, n = 65 trials, L2, n= 65 trials, L3, n = 65
901 trials, L4, n = 65 trials, L5, n = 70 trials from 4 mice.

902 **(E)** *Left*: Latency to approach reward in seconds for pPVT$^{D2(+)}$ terminals across latency
903 blocks. Repeated measures ANOVA, ****$p<0.0001$. *Right*: Velocity (m/s) during reward
904 approach calculated across each latency block. Repeated measures ANOVA,
905 ****$p<0.0001$.
906 **(F)** *Left*: Average GCaMP6s pPVT$^{D2(+)}$ terminal dynamics for fast approach (L1) and
907 slow approach (L5). The red line indicates 20-80% of the slope of the line. *Right*: Slope-
908 of-the-line quantifications of GCaMP6s activity from PVT$^{D2(+)}$ terminals across approach
909 latency blocks. Repeated measures ANOVA, *$p<0.05$.
910 **(G)** Correlation between the approach latency and the slope-of-the-line quantifications
911 of GCaMP6s responses during reward approach in pPVT$^{D2(+)}$ terminals.
912 **(H)** Correlation between the approach velocity and the slope-of-the-line during the
913 reward approach.
914 **(I)** AUC quantification of the reward approach-evoked changes in GCaMP6s activity
915 across approach latency blocks. Repeated measures ANOVA, $p=0.52$; ns, not
916 significant.
917 **(J)** Same as (D) but sorted by trial order and binned into 5 'trial group blocks' (G1-G5).
918 Yellow dots represent reward zone arrival.
919 **(K)** *Left*: Latency to approach reward in seconds for pPVT$^{D2(+)}$ terminals across latency
920 blocks. Repeated measures ANOVA, ****$p<0.0001$. *Middle*: Average GCaMP6s
921 approach dynamics of pPVT$^{D2(+)}$ terminals comparing approach trials performed early
922 and late in the session. *Right*: Max peak quantification of the approach-evoked changes
923 in GCaMP6s activity from pPVT$^{D2(+)}$ terminals across trial group blocks. Repeated
924 measures ANOVA, $p=0.37$; ns, not significant.

925 **(L)** *Left*: Average GCaMP6s responses from pPVT$^{D2(+)}$ terminals during trial termination
926 and return. *Right*: Quantification of the return-evoked changes in GCaMP6s
927 fluorescence in pPVT$^{D2(+)}$ terminals. AUC, two-tailed paired t-test, *$p<0.05$.
928 **(M)** *Left*: Schematic of stereotaxic injections and fiber implantation. *Right:*
929 Representative images of GCaMP6s expression in D2(-) neurons in the aPVT and fiber
930 placement in NAc.
931 **(N)** *Left*: Average GCaMP6s approach-evoked responses from aPVT$^{D2(-)}$ terminals
932 during the reward approach. *Right*: Quantification of the approach-evoked changes in
933 GCaMP6s in aPVT$^{D2(-)}$ terminals. AUC, n = 646 trials from 6 mice, two-tailed paired t-
934 test, **$p<0.01$.
935 **(O)** *Left*: Average GCaMP6s responses from aPVT$^{D2(-)}$ terminals during reward delivery.
936 *Right*: Quantification of reward-evoked changes in GCaMP6s. AUC, two-tailed paired t-
937 test, **$p<0.01$.
938 **(P)** Heatmap showing inhibitory approach responses from aPVT$^{D2(-)}$ terminals, time-
939 locked to cue onset, sorted by latency to approach the reward zone, and binned into 5
940 'approach latency blocks' (L1 – L5). L1, n = 127 trials, L2, n= 129 trials, L3, n = 127
941 trials, L4, n = 130 trials, L5, n = 133 trials from 6 mice.
942 **(Q)** *Left*: Latencies to reach the reward zone in seconds for each approach latency
943 block. Repeated measures ANOVA, ****$p = 0.0001$. *Right*: Velocity (m/s) during reward
944 approach calculated for each approach latency block. Repeated measures ANOVA,
945 ****$p<0.0001$.
946 **(R)** Average GCaMP6s dynamics for aPVT$^{D2(-)}$ terminals during fast and slow trials.

947 **(S)** Slope-of-the-line quantifications of GCaMP6s activity from aPVT$^{D2(-)}$ terminals across
948 approach latency blocks. Repeated measures ANOVA, *p=0.42*; ns, not significant.
949 **(T)** *Left*: No correlation between the approach latency and the slope-of-the-line
950 quantifications of GCaMP6s responses from aPVT$^{D2(-)}$ terminals during the approach.
951 *Right*: No correlation between approach velocity and the slope-of-the-line quantifications
952 of GCaMP6s responses during the reward approach.
953 **(U)** AUC quantification of the approach-evoked changes in GCaMP6s activity across
954 approach latency blocks. Repeated measures ANOVA, *p=0.11;* ns, not significant. ns,
955 not significant.
956 **(V)** *Left*: Same as (P), but responses were sorted by trial order and binned into 5 'trial
957 group blocks' (G1 – G5). Yellow dots represent reward zone arrival. *Right*: Latencies to
958 reach reward across trial group blocks for aPVT$^{D2(-)}$ terminals. Repeated measures
959 ANOVA, ***$p<0.001$.
960 **(W)** *Left*: Average GCaMP6s aPVT$^{D2(-)}$ terminal dynamics comparing trials performed
961 early and late in the session. *Right*: AUC quantification of the approach-evoked changes
962 in GCaMP6s activity from aPVT$^{D2(-)}$ terminals across trial group blocks. Repeated
963 measures ANOVA, *p=0.26*; ns, not significant.
964 **(X)** *Left*: Average GCaMP6s responses from aPVT$^{D2(-)}$ terminals during trial termination
965 and return. *Right*: Quantification of the return-evoked changes in GCaMP6s
966 fluorescence in aPVT$^{D2(-)}$ terminals. AUC, two-tailed paired t-test, *$p<0.05$.
967 All data in the figure are shown as mean ±s.e.m.
968

969 **Supplemental Figure 1. Mice performance in foraging–like task to characterize**
970 **motivated behavior in rodents and trial distribution per experimental group.**
971 **(A).** Schematics depicting our foraging-like reward-seeking task.
972 **(B)** Quantification of trials completed during the first days of training (Days 1-2) and the
973 last days of training (Days 13-14) for all the mice included in the study. Two-tailed
974 paired t-test, ****$p<0.0001$.
975 **(C)** *Left:* Comparisons of the latencies to the reward zone. Lighter colors indicate the
976 first days of training, and darker colors indicate the last days of training. *Middle:*
977 Comparison of the latencies to reward zone between equivalent trials for training days
978 1-2 and days 13-14 (approx. 20 first trials). Right: Quantifications of (*Middle*). Two-tailed
979 paired t-test, to zone ****$p<0.0001$.
980 **(D)** Same as (C) but for latencies to reward delivery. Two-tailed paired t-test, to delivery
981 ***$p<0.001$.
982 **(E)** Same as (D) but for latencies to next trial. Two-tailed paired t-test, to next trial
983 ****$p<0.0001$.
984 **(F)** *Left:* Comparison of all trials completed during testing with those included in the
985 photometry analysis. On average, approximately ten trials were excluded per testing
986 session. Two-tailed paired t-test, ****$p<0.0001$. *Middle:* Plots showing average latencies
987 to the reward zone throughout the testing session for trials included in the photometry
988 analysis. *Right:* Same as (Middle) but for latencies to reward delivery.
989 **(G)** Pie charts showing the trial distribution per both approach latency blocks (L1-L5)
990 and trial group blocks (G1-G5).

991 **(H)** Pie chart showing individual trial contribution per animal for all groups tested in the
992 study (pPVT$^{D2(+)}$, pPVT$^{D2(-)}$, aPVT$^{D2(-)}$, pPVT$^{D2(+)}$ -NAc terminals, aPVT$^{D2(-)}$ -NAc
993 terminals).
994 **(I)** *Left:* Density estimates plots for trials during pPVT$^{D2(+)}$ neuronal imaging and sorted
995 by approach latency blocks. *Right*: Trial distribution for those trials performed during
996 pPVT$^{D2(+)}$ neuronal imaging showing proportion of trials in approach latency blocks and
997 their distribution across trial group blocks.
998 **(J)** *Left:* Density estimates graphs for trials during pPVT$^{D2(+)}$ neuronal imaging and
999 sorted by trial group blocks. *Right*: Trial distribution for those trials performed during
1000 pPVT$^{D2(+)}$ neuronal imaging showing proportion of trials in trial group blocks and their
1001 distribution across approach latency blocks.
1002 **(K)** Same as (I) but for trials during pPVT$^{D2(-)}$ neuronal imaging.
1003 **(L)** Same as (J) but for trials during pPVT$^{D2(-)}$ neuronal imaging.
1004 All data in the figure are shown as mean ±s.e.m.
1005
1006 **Supplementary Figure 2. *In vivo* dynamics of PVT$^{D2(+)}$ and PVT$^{D2(-)}$ neurons during**
1007 **cue presentation and during reward omission testing session.**
1008 **(A)** *Left:* Average approach-evoked GCaMP6s responses of pPVT$^{D2(+)}$ neurons during
1009 cue presentation. *Right:* AUC quantification of baseline and cue activity of pPVT$^{D2(+)}$
1010 neurons. Two-tailed paired t-test, $p=0.82$; ns, not significant.
1011 **(B)** *Left:* Average GCaMP6s responses of pPVT$^{D2(+)}$ neurons during cue presentation
1012 grouped by approach latency blocks. *Right:* AUC quantifications of GCaMP6s activity

1013 from pPVT$^{D2(+)}$ neurons across approach latency blocks. Repeated measures ANOVA,
1014 *p=0.19;* ns, not significant.
1015 **(C)** Same as (B) but grouped by trial group blocks. Repeated measures ANOVA,
1016 **p<0.05;* G1 vs. G5 Tukey's multiple comparisons test, *p=0.13*.
1017 **(D)** *Left:* Average approach-evoked GCaMP6s responses of pPVT$^{D2(+)}$ neurons in the
1018 OM session. *Middle Left:* AUC quantification of baseline and approach activity of
1019 pPVT$^{D2(+)}$ neurons in the OM session. Two-tailed paired t-test, ***p<0.01*. *Middle Right:*
1020 Heatmap of GCaMP6s responses from pPVT$^{D2(+)}$ neurons during approach in the OM
1021 session. GCaMP6s responses were time-locked to cue onset, and trials were sorted by
1022 trial order and binned into 5 'trial group blocks' (G1 – G5). *Right:* AUC quantification
1023 comparing approach-evoked GCaMP6s responses of pPVT$^{D2(+)}$ neuronal responses
1024 between rewarded (Rew) and unrewarded (OM) testing sessions. Two-tailed unpaired t-
1025 test ***p<0.01.*
1026 **(E)** *Left:* Average pPVT$^{D2(+)}$ neuronal GCaMP6s responses when mice entered the food
1027 port but were not rewarded. *Right:* AUC quantification of the reward omission-evoked
1028 changes in GCaMP6s fluorescence in pPVT$^{D2(+)}$ neurons. Two-tailed paired t-test,
1029 *p=0.24*; ns, not significant.
1030 **(F)** *Left:* Latencies to reach the reward zone across trial group blocks. Repeated
1031 measures ANOVA, *p=0.26;* ns, not significant. *Middle:* Average pPVT$^{D2(+)}$ GCaMP6s
1032 responses during approach in the OM session for early and late trials. *Right:* AUC
1033 quantification of pPVT$^{D2(+)}$ GCaMP6s activity in the OM session for trial group blocks.
1034 Repeated measures ANOVA, *p =0.71*; ns, not significant.

1035 **(G)** Same as (F) but for pPVT$^{D2(+)}$ during reward omission. Repeated measures ANOVA,
1036 *p=0.44*; ns, not significant.
1037 **(H)** *Left:* Latencies to reach the reward zone in seconds for each approach latency block
1038 during the reward omission session. Repeated measures ANOVA, ***p<0.0001. Middle:*
1039 Average pPVT$^{D2(+)}$ neuronal GCaMP6s responses for fast and slow reward approach in
1040 the OM session. The red line indicates 20-80% of the slope of the line. *Right:* In the OM
1041 session, slope-of-the-line quantifications of pPVT$^{D2(+)}$ neuronal GCaMP6s activity across
1042 approach latency blocks. Repeated measures ANOVA, ***p<0.01*.
1043 **(I)** Slope-of-the-line quantifications of pPVT$^{D2(+)}$ neuronal GCaMP6s activity comparing
1044 latencies during fast approach (L1) and slow approach (L5) between rewarded (Rew)
1045 and unrewarded (OM) testing sessions. L1- two-tailed unpaired t-test, *p=0.97*; ns, not
1046 significant. L5- two-tailed unpaired t-test, *p= 0.65*; ns, not significant.
1047 **(J)** *Left:* Average approach-evoked GCaMP6s responses of pPVT$^{D2(-)}$ neurons during
1048 cue presentation. *Right:* AUC quantification of baseline and cue activity of pPVT$^{D2(-)}$
1049 neurons. Two-tailed paired t-test, *p=0.67*; ns, not significant.
1050 **(K)** *Left:* Average GCaMP6s responses of pPVT$^{D2(-)}$ neurons during cue presentation
1051 grouped by approach latency blocks. *Right:* AUC quantifications of GCaMP6s activity
1052 from pPVT$^{D2(-)}$ neurons across approach latency blocks. Repeated measures ANOVA,
1053 **p<0.05;* L1 vs. L5 Tukey's multiple comparisons test, *p=0.06*.
1054 **(L)** Same as (K) but grouped by trial group blocks. Repeated measures ANOVA,
1055 *p=0.50*; ns, not significant.

1056 **(M)** *Left:* Average approach-evoked GCaMP6s responses of aPVT$^{D2(-)}$ neurons during
1057 cue presentation. *Right:* AUC quantification of baseline and cue activity of aPVT$^{D2(-)}$
1058 neurons. Two-tailed paired t-test, ***p<0.01*.
1059 **(N)** *Left:* Average GCaMP6s responses of aPVT$^{D2(-)}$ neurons during cue presentation
1060 grouped by approach latency blocks. *Right:* AUC quantifications of GCaMP6s activity
1061 from aPVT$^{D2(-)}$ neurons across approach latency blocks. Repeated measures ANOVA,
1062 *p=0.19*; ns, not significant.
1063 **(O)** Same as (N) but grouped by trial group blocks. Repeated measures ANOVA,
1064 *p=0.53*; ns, not significant.
1065 All data in the figure are shown as mean ±s.e.m.
1066
1067 **Supplementary Figure 3. *In vivo* dynamics of PVT$^{D2(+)}$ and PVT$^{D2(-)}$ neurons and**
1068 **terminals using the novel FLMM analysis during distinct trial events.**

1069 **(A)** FLMM coefficient estimates plots of the approach latency effect and statistical
1070 significance at each trial time-point results for the photometric responses of pPVT$^{D2(+)}$
1071 neurons for cue presentation and reward zone entry. No association between pPVT$^{D2(+)}$
1072 GCaMP6s responses and approach latency at cue presentation (*left*) nor at reward
1073 zone entry (*right*).

1074 **(B)** FLMM coefficient estimates plots of the approach trial order effect and statistical
1075 significance at each trial time-point results for the photometric responses of pPVT$^{D2(+)}$
1076 neurons for cue presentation and reward zone entry. The plots show a negative
1077 association between pPVT$^{D2(+)}$ GCaMP6s responses and trial order right after cue
1078 presentation (*left*) and before reward zone entry (*right*).

1079 **(C)** Same as (A) but for photometric responses of pPVT$^{D2(-)}$ neuron. No association
1080 between pPVT$^{D2(-)}$ GCaMP6s responses and approach latency at cue presentation (*left*)
1081 or at reward zone entry (*right*).

1082 **(D)** Same as (B) but for photometric responses of pPVT$^{D2(-)}$ neuron. No association
1083 between pPVT$^{D2(-)}$ GCaMP6s responses and trial order at cue presentation (*left*) nor at
1084 reward zone entry (*right*).

1085 **(E)** Same as (A) but for photometric responses of aPVT$^{D2(-)}$ neurons. No association
1086 between aPVT$^{D2(-)}$ GCaMP6s responses and approach latency at cue presentation (*left*)
1087 or at reward zone entry (*right*).

1088 **(F)** Same as (B) but for photometric responses of aPVT$^{D2(-)}$ neurons. No association
1089 between aPVT$^{D2(-)}$ GCaMP6s responses and trial order at cue presentation (*left*) nor at
1090 reward zone entry (*right*).

1091 **(G)** FLMM coefficient estimates plots applying 'recording location' (i.e., aPVT or pPVT)
1092 as a covariate and showing statistical significance at each trial time-point results for the
1093 photometric responses of PVT$^{D2(-)}$ neurons for cue presentation and reward zone entry.
1094 No statistically significant differences between aPVT$^{D2(-)}$ GCaMP6s responses and
1095 pPVT$^{D2(-)}$ GCaMP6s responses at cue presentation (*left*) nor at reward zone entry
1096 (*right*).

1097 **(H)** FLMM coefficient estimates plots of the return latency effect and statistical
1098 significance at each trial time-point results for the photometric responses of pPVT$^{D2(+)}$
1099 neurons for trial termination and trigger zone entry. No association between pPVT$^{D2(+)}$

1100 GCaMP6s responses and return latency at trial termination (*left*) nor at trigger zone
1101 entry (*right*).

1102 **(I)** FLMM coefficient estimates plots of the return trial order effect and statistical
1103 significance at each trial time-point results for the photometric responses of $pPVT^{D2(+)}$
1104 neurons for trial termination and trigger zone entry. No association between $pPVT^{D2(+)}$
1105 GCaMP6s responses and trial order at trial termination (*left*) nor at trigger zone entry
1106 (*right*).

1107 **(J)** Same as (H) but for photometric responses of $pPVT^{D2(-)}$ neuron. No association
1108 between $pPVT^{D2(-)}$ GCaMP6s responses and return latency at trial termination (*left*) nor
1109 at trigger zone entry (*right*).

1110 **(K)** Same as (I) but for photometric responses of $pPVT^{D2(-)}$ neuron. No association
1111 between $pPVT^{D2(-)}$ GCaMP6s responses and trial order at trial termination (*left*) nor at
1112 trigger zone entry (*right*).

1113 **(L)** Same as (H) but for photometric responses of $aPVT^{D2(-)}$ neuron. No association
1114 between $aPVT^{D2(-)}$ GCaMP6s responses and return latency at trial termination (*left*) nor
1115 at trigger zone entry (*right*).

1116 **(M)** Same as (I) but for photometric responses of $aPVT^{D2(-)}$ neuron. No association
1117 between $aPVT^{D2(-)}$ GCaMP6s responses and trial order at trial termination (*left*) nor at
1118 trigger zone entry (*right*).

1119 **(N)** FLMM coefficient estimates plots applying 'recording location' (i.e., aPVT or pPVT)
1120 as a covariate and showing statistical significance at each trial time-point results for the
1121 photometric responses of $PVT^{D2(-)}$ neurons for trial termination and trigger zone entry.

1122 No statistically significant differences between aPVT$^{D2(-)}$ GCaMP6s responses and
1123 pPVT$^{D2(-)}$ GCaMP6s responses at trial termination (*left*) nor at trigger zone entry (*right*).

1124 **(O)** FLMM coefficient estimates plots of the approach latency effect and statistical
1125 significance at each trial time-point results for the photometric responses of pPVT$^{D2(+)}$
1126 terminals for cue presentation and reward zone entry. *Left:* No association between
1127 pPVT$^{D2(+)}$ terminal responses and approach latency at cue presentation. *Right:* Plot
1128 showing a negative association between pPVT$^{D2(+)}$ terminal responses and approach
1129 latency before reward zone entry.

1130 **(P)** FLMM coefficient estimates plots of the approach trial order effect and statistical
1131 significance at each trial time-point results for the photometric responses of pPVT$^{D2(+)}$
1132 terminals for cue presentation and reward zone entry. *Left:* No association between
1133 pPVT$^{D2(+)}$ terminal responses and trial order at cue presentation. *Right:* Plot showing a
1134 negative association between pPVT$^{D2(+)}$ terminal responses and trial order
1135 approximately 1 sec after reward zone entry.

1136 **(Q)** Same as (O) but for photometric responses of aPVT$^{D2(-)}$ terminals. *Left:* No
1137 association between aPVT$^{D2(-)}$ terminal responses and approach latency at cue
1138 presentation. *Right:* Plot showing a positive association between aPVT$^{D2(-)}$ terminal
1139 responses and approach latency before reward zone entry.

1140 **(R)** Same as (P) but for photometric responses of aPVT$^{D2(-)}$ terminals. No association
1141 between aPVT$^{D2(-)}$ terminal responses and trial order at cue presentation (*left*) nor at
1142 reward zone entry (*right*).

1143 **(S)** FLMM coefficient estimates plots of the return latency effect and statistical
1144 significance at each trial time-point results for the photometric responses of $pPVT^{D2(+)}$
1145 terminals for trial termination and trigger zone entry. *Left:* No association between
1146 $pPVT^{D2(+)}$ terminal responses and return latency at trial termination. *Right:* Plot showing
1147 a positive association between $pPVT^{D2(+)}$ terminal responses and return latency before
1148 trigger zone entry.

1149 **(T)** FLMM coefficient estimates plots of the return trial order effect and statistical
1150 significance at each trial time-point results for the photometric responses of $pPVT^{D2(+)}$
1151 terminals for trial termination and trigger zone entry. *Left:* Plot showing a positive
1152 association between $pPVT^{D2(+)}$ terminal responses and return trial order approx. 1 sec
1153 after trial termination. *Right:* No association between $pPVT^{D2(+)}$ terminal responses and
1154 return trial order during trigger zone arrival.

1155 **(U)** Same as (S) but for photometric responses of $aPVT^{D2(-)}$ terminals. *Left:* No
1156 association between $aPVT^{D2(-)}$ terminal responses and return latency at trial termination.
1157 *Right:* Plot showing a negative association between $aPVT^{D2(-)}$ terminal responses and
1158 return latency before trigger zone entry.

1159 **(V)** Same as (T) but for photometric responses of $aPVT^{D2(-)}$ terminals. No association
1160 between $aPVT^{D2(-)}$ terminal responses and return trial order at trial termination (*left*) nor
1161 at trigger zone entry (*right*).

1162

1163 **Supplementary Figure 4. Optical fiber placements.**

1164 **(A)** Fiber implant location in the pPVT for D2(+) photometry recordings used for

1165 experiments in Fig. 1- $pPVT^{D2(+)}$.

1166 **(B)** Fiber implant location in pPVT for GFP controls used in experiments in Fig. 1.

1167 **(C)** Fiber implant location in the pPVT for D2(-) photometry recordings used in

1168 experiments in Fig. 2 - $pPVT^{D2(-)}$.

1169 **(D)** Fiber implant location in the aPVT for D2(-) photometry recordings used for

1170 experiments in Fig. 2 - $aPVT^{D2(-)}$.

1171 **(E)** NAc fiber implants for $pPVT^{D2(+)}$ terminal photometry recordings used for

1172 experiments in Fig. 4A-L.

1173 **(F)** NAc fiber implants for $aPVT^{D2(-)}$ terminal photometry recordings used for experiments

1174 in Fig. 4M-X.

1175 **METHODS**

1176 **Mice**

1177 For all experiments, both male and female *Drd2*-Cre mice (8–15 weeks of age) were
1178 used. These mice were obtained from the GENSAT (founder line ER44) and were group-
1179 housed under a 12-h light-dark cycle (6 a.m. to 6 p.m. light) at a temperature of 70–74 °F
1180 and 40–65% humidity. After surgery, mice were single-housed and were provided with
1181 food and water *ad-libitum.* Food was restricted for two days before initiating behavioral
1182 training procedures, and mice were fed accordingly to maintain 85% of their free-feeding
1183 weight. After all testing was completed, mice returned to *ad-libitum* feeding. Animals were
1184 randomly allocated to the different experimental conditions reported in this study. Notably,
1185 all procedures were performed in accordance with the *Guide for the Care and Use of*
1186 *Laboratory Animals* and were approved by the National Institute of Mental Health (NIMH)
1187 Animal Care and Use Committee.

1188 **Viral vectors**

1189 AAV9-hSyn-FLEX-GCaMP6s-WPRE-SV40 was produced by the Vector Core of the
1190 University of Pennsylvania. AAV9-CAG-Flex-GFP was produced by the University of
1191 North Carolina, Chapel Hill (UNC) Vector Core. AAV9-Syn-DO-GCaMP6s was produced
1192 by Charu Ramakrishnan (Deisseroth laboratory, Stanford University, CA, USA).

1193 **Stereotaxic surgery**

1194 Mice were first anesthetized with a Ketamine/Xylazine solution, and an AngleTwo
1195 stereotaxic device (Leica Biosystems) was used for viral injections (approximately one µl)

1196 at the following stereotaxic coordinates (at a 6°angle): pPVT, −1.60 mm from Bregma,
1197 0.06 mm lateral from midline, and −3.30 mm vertical from the cortical surface; aPVT,
1198 −0.30 mm from bregma, 0.00 mm lateral from the midline and −4.30 mm vertical from the
1199 cortical surface. For the fiber photometry experiments, optical fibers with diameters of 400
1200 μm (0.66 NA - Doric Lenses) were used. These fibers were implanted over the pPVT or
1201 aPVT immediately following viral injections (targeted 300-400 μm above the injection
1202 site). NAc fibers coordinates were: 1.40 mm from bregma, 0.70 mm lateral from the
1203 midline, and −4.80 mm vertical from the cortical surface. Fibers were cemented using
1204 C&B Metabond Quick Adhesive Cement System (Parkell, Inc.) and Jet Brand dental
1205 acrylic (Lang Dental Manufacturing Co., Inc.). For analgesia and anti-inflammatory
1206 purposes postoperatively, mice received subcutaneous injections with metacam
1207 (meloxicam, 1–2 mg/kg) and were allowed to recover on a heating pad, where they were
1208 constantly monitored. Following stereotaxic injections, AAVs were allowed for 2–3 weeks
1209 for maximal expression.

1210 **Foraging-like reward-seeking task**

1211 The foraging track consisted of a linear maze (150 × 32 × 25, L ×W× H in cm) containing
1212 digital distance sensors (15 cm, Pololu Robotics, and Electronics) located throughout the
1213 track, which allowed us to track the movement of the mice through the maze. The maze
1214 consisted of three zones: trigger zone, corridor, and reward zone. The opposite ends of
1215 the track were designated as the trigger zone and reward zone and were connected by a
1216 long corridor. Training in the task consisted of two initial sessions of magazine training, in
1217 which ¾ of the maze was closed, and mice received 100 μls of the reward every minute

1218 for 60 mins. After that, mice were trained in the task for at least 14 days until they reliably
1219 performed at least 50 trials or more. The task consisted of 60 min-long sessions of self-
1220 paced trials, and mice received one testing session per day. Food-restricted mice were
1221 trained to wait in the trigger zone for two seconds for each trial. An auditory cue was then
1222 presented, which signaled reward availability, allowing mice to run from the trigger zone,
1223 down the corridor, and into the reward zone to retrieve a food reward (strawberry
1224 Ensure®). Delivery and food consumption signaled trial termination, and therefore, mice
1225 had to return to the trigger zone to initiate another trial. Experimental schedule and data
1226 acquisition were implemented through the Abet II software for operant control (Lafayette
1227 Instruments Neuroscience) and through the Whisker multimedia software (Lafayette
1228 Instruments Neuroscience).

1229 **Bulk Ca^{2+} and fiber photometry**

1230 All photometry experiments were performed using an RZ5P acquisition system (Tucker-
1231 Davis Technologies; TDT) equipped with a real-time signal processor and controlled by
1232 a software interface (Synapse version 92). Specifically, the system is integrated with two
1233 continuous sinusoidally modulated LEDs (DC4100, ThorLabs) at 473 nm (211 Hz) and
1234 405 nm (531 Hz) that serve as the light source to excite GCaMP6s and an isosbestic
1235 autofluorescence signal, respectively. The LED intensity (ranging from 10–15 μW) at the
1236 interface between the fiber tip and the animal was constant throughout the session.
1237 Fluorescence signals were collected by the same fiber implant that was coupled to a 400
1238 μm optical patch-cord (0.48 NA) and focused onto two separate photoreceivers (2151,
1239 Newport Corporation) connected to the emission ports of a custom-ordered fiber

1240 photometry Mini Cube (Doric Lenses). TTL pulses recorded by the same system were
1241 used to annotate the occurrence of behavioral manipulations. For the measurements of
1242 fluorescent calcium signals and ΔF/F analysis, a least-squares linear fit to the 405 nm
1243 signal to align it to the 470 nm signal was first applied. The resulting fitted 405 nm signal
1244 was then used to normalize the 473 nm as follows: ΔF/F = (473 nm signal − fitted 405 nm
1245 signal)/fitted 405 nm signal. All GCaMP6s signal data is presented as the z-score of the
1246 dF/F from a baseline prior to the onset of events.

1247 ***In-vivo dynamics analyses***

1248 Upon calculating the z-score of the dF/F for each event in every trial the mice performed,
1249 the latency to the reward zone was calculated. All trials that were higher than 11 seconds
1250 and the events corresponding to the trial (cue, approach, reward zone arrival, reward
1251 delivery, and consumption) were excluded. Approximately more than 75% of the trials
1252 met this inclusion criterion (Supp. Fig. 1F). After that, the trials and events for each
1253 individual testing session were sorted by either their latency to approach the reward zone
1254 (Approach Latency Blocks) or by trial order - the time in which the trial was completed
1255 within a testing session (Trial Group Blocks). After sorting the trials in each testing
1256 session, these were then divided into 5 equivalent trial blocks.

1257 Slope-of-the-line calculations: Activity traces for reward approach and reward termination
1258 included the activity from time 0, which corresponded to cue delivery, to 11 sec, which
1259 was our cut-off for included trials. The maximum and minimum peaks were calculated for
1260 each trace, and 80% and 20% values of the max or min peaks were determined.
1261 Thereafter, the slope-of-the-line was fitted for the corresponding 80% and 20% values.

1262 **Functional Linear Mixed Model Encoder (FLMM)**

1263 The basis for the FLMM analysis was previously described in detail[23]. Briefly, the FLMM
1264 analysis is a statistical framework that combines linear mixed models (LMM) and
1265 functional regression. The LMM portion of the analysis is a statistical method for data that
1266 contains repeated measures and tests the association between independent factors or
1267 covariates and dependent factors or outcomes. As such, the LMM allows for the analysis
1268 of nested experiments, such as those that contain multiple stimuli and behaviors. The
1269 LMM analyses are then combined with functional regression, which takes advantage of
1270 autocorrelations in the signal and allows for the calculation of the joint 95% coefficient
1271 intervals (CIs) that can be used as the equivalent of other familiar statistical tests (e.g.,
1272 ANOVAs, correlations). The FLMM framework outputs a plot for each covariate in the
1273 model (i.e., the effects of latency and the effects of trial order) and shows whether these
1274 are significantly associated with the photometry signal at each time point during the
1275 behavior. These FLMM output plots consist of the regression coefficient estimates
1276 associated with each covariate at a particular point in the trial (solid lines). The plots also
1277 show the estimated covariance function using a pointwise 95% CI for the coefficients of
1278 each point (dark-shaded area). Lastly, the plot also shows the calculated joint 95% CI
1279 (light-shaded area), which allows for the joint interpretations of each covariate effect on
1280 the photometry signals across time intervals at multiple locations in the trial along the
1281 functional domain. Statistical significance for the effect of a covariate on the photometry
1282 signal can be readily observed in these output plots. As such, the points in the plot where
1283 pointwise CI does not contain zero indicate the pointwise statistical significance, and the
1284 points where the joint CI does not contain zero indicate jointly statistical significance.

1285 **Histology**

1286 To verify GCaMP6s expression and optical fiber placements, mice were injected with
1287 euthanasia solution and subsequently sacrificed via transcardial perfusion, first with PBS
1288 and then with paraformaldehyde (PFA; 4% in PBS). Brains were then post-fixed in 4%
1289 PFA at 4 °C overnight and cryoprotected using a 30% PBS-buffered sucrose solution for
1290 ~24–36 h. Coronal brain sections (45 μm) were generated using a freezing microtome
1291 (SM 2010R, Leica). Images were taken using a Carl Zeiss LSM 780 confocal microscope
1292 running ZEN software (version 2.3, Carl Zeiss Microscopy, LLC). Optical fiber placements
1293 for all subjects included in this study are presented in Supplemental Fig. 4. Mice without
1294 correct targeting of optical fibers or GCaMP6s expression were excluded from this study.
1295 Correct viral expression for $pPVT^{D2(+)}$ neurons was determined by following the D2R
1296 expression reported in our previous studies[4,16]. Correct optical fiber placement was
1297 assessed by whether the tip of the fiber was immediately above the pPVT, as shown in
1298 Fig. 1A. No animals were excluded from this group. Correct viral expression for $PVT^{D2(-)}$
1299 also followed the D2R(-) expression shown in our previous studies[16]. Particularly for
1300 pPVT, any animals that showed virus expression in the medial or lateral habenular or in
1301 the ventral medial dorsal thalamus were excluded. For aPVT, any animal that showed
1302 virus expression in the paretenial thalamus was excluded from the study. For these
1303 animals, correct optical placement was again assessed by whether the tip of the fiber was
1304 immediately above pPVT or aPVT, respectively. For the $pPVT^{D2(-)}$ group, one mouse
1305 was excluded for incorrect virus expression, and for the $aPVT^{D2(-)}$ group, four mice were
1306 excluded for incorrect virus expression and incorrect optical fiber placement.
1307

1308 **Statistics and data presentation**

1309 All data were analyzed using GraphPad Prism (Domatics) and Origin Pro 2016 (OriginLab
1310 Corp). **The FLMM analysis used R Studio and the 'FastFLMM' and 'ggplot2'**
1311 **packages.** All statistical tests are indicated when used. No assumptions or corrections
1312 were made prior to data analysis. For statistical analyses, a two-tailed paired t-test
1313 (nonparametric; test statistic: t) and a repeated measures ANOVA (nonparametric; test
1314 statistic: F) were used. ANOVA was followed by a post-hoc Tukey multiple comparisons
1315 test if the omnibus test detected a significant difference. All data are presented as mean
1316 ± s.e.m. The sample sizes used in our study are similar to those of prior studies[10]. For all
1317 the groups tested, the sample size was at least 6 mice, with the exception of the terminal
1318 imaging of $pPVT^{D2(+)}$ neurons, for which there were 4 mice. (Supp. Fig. 1H). This was due
1319 to technical challenges associated with performing calcium imaging from terminals in our
1320 task. All experiments were replicated at least once. The data were assumed to be normal,
1321 but this was not formally tested.

1322 **Data availability**

1323

1324 All the data that support the findings presented in this study are available from the
1325 corresponding author upon reasonable request.

1326 Figure 1

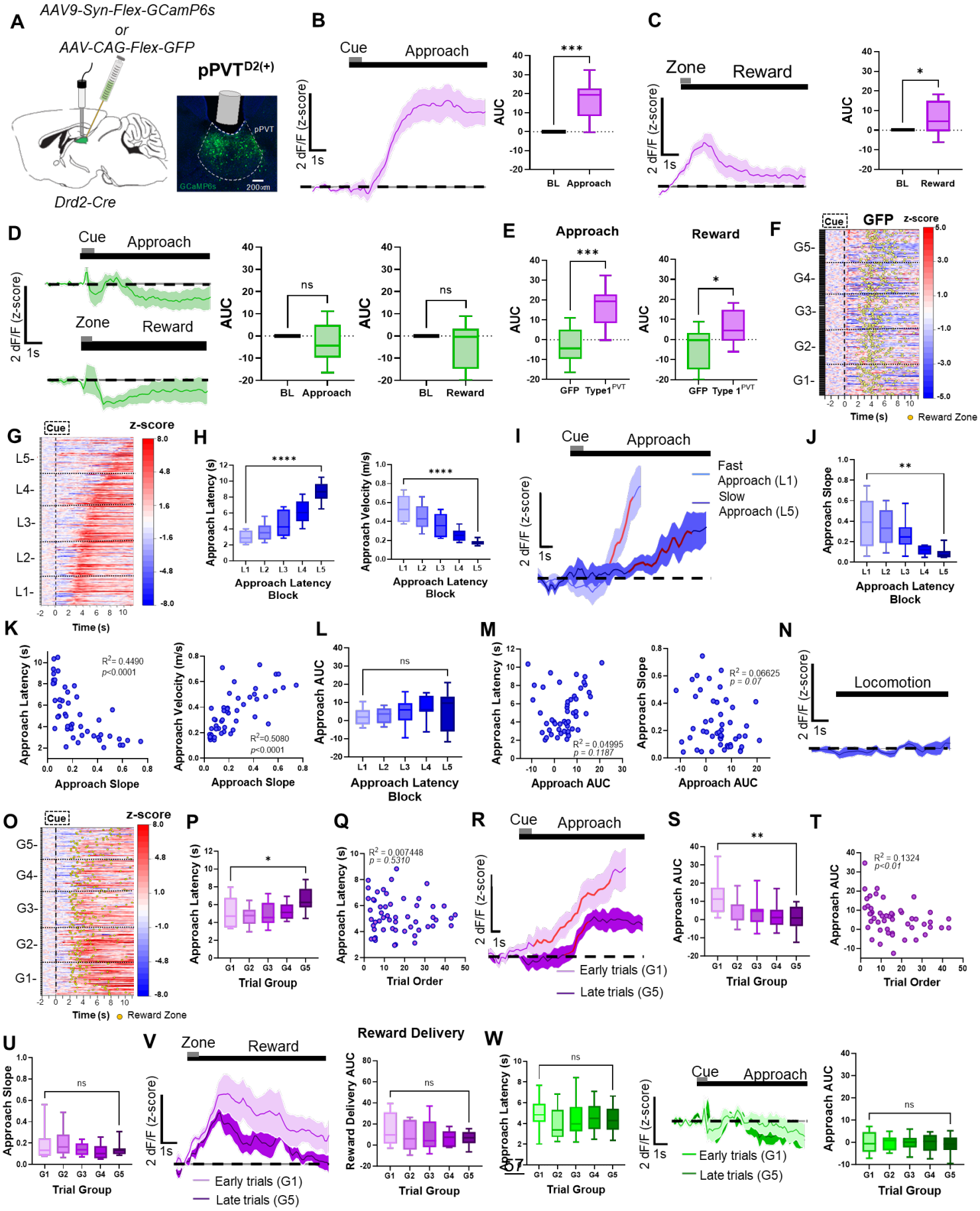

1327 Figure 2

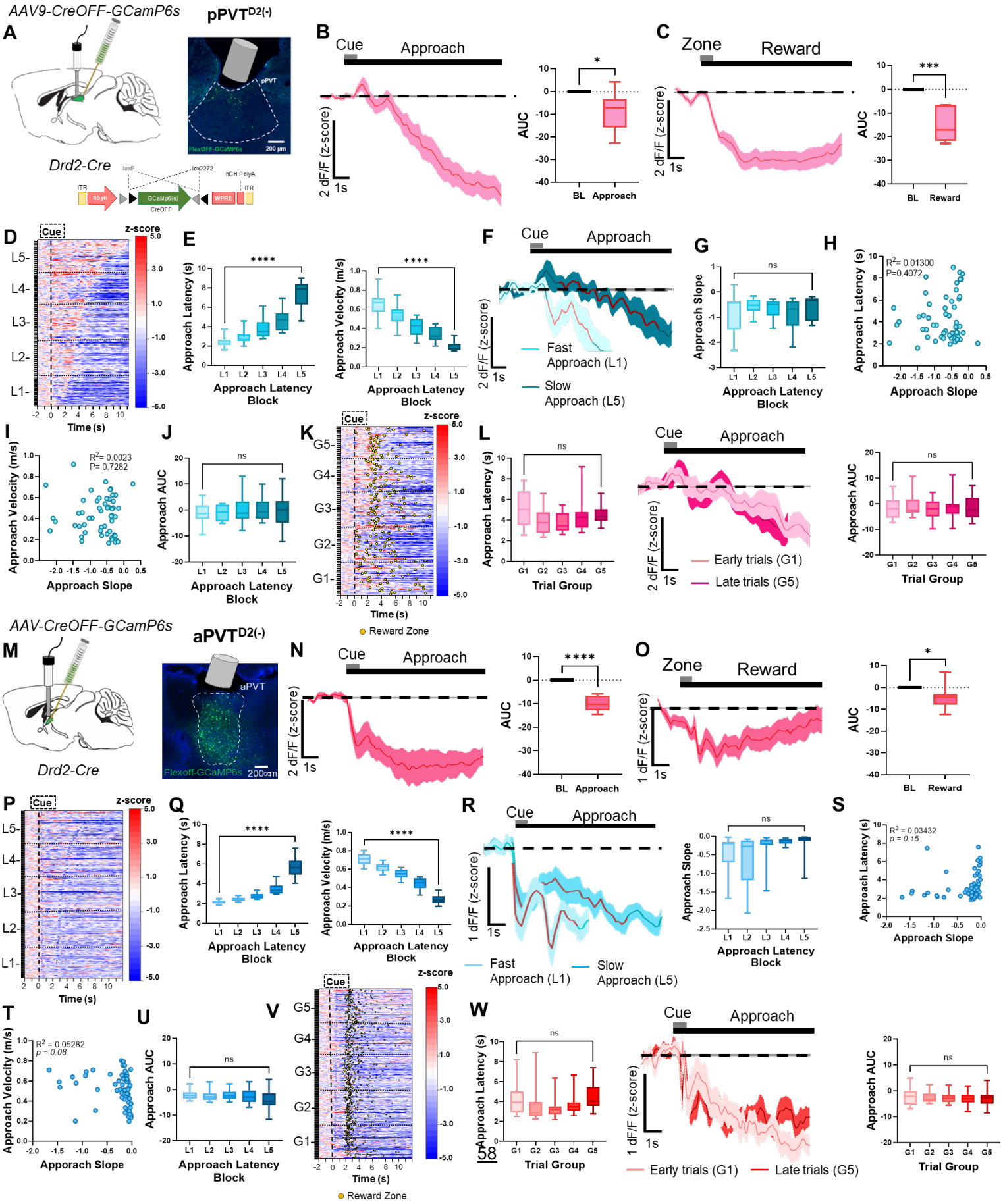

1328 Figure 3

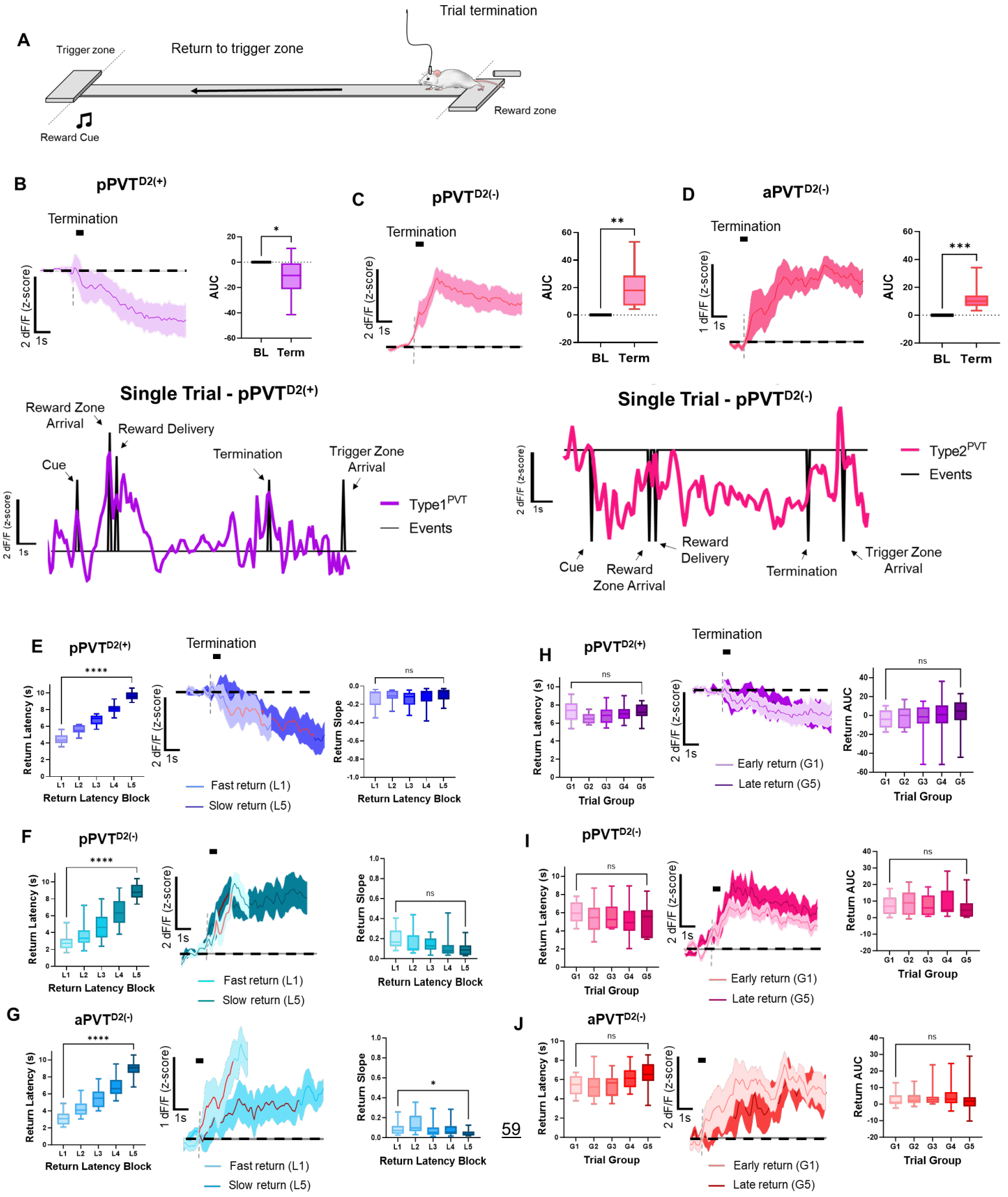

1329 Figure 4

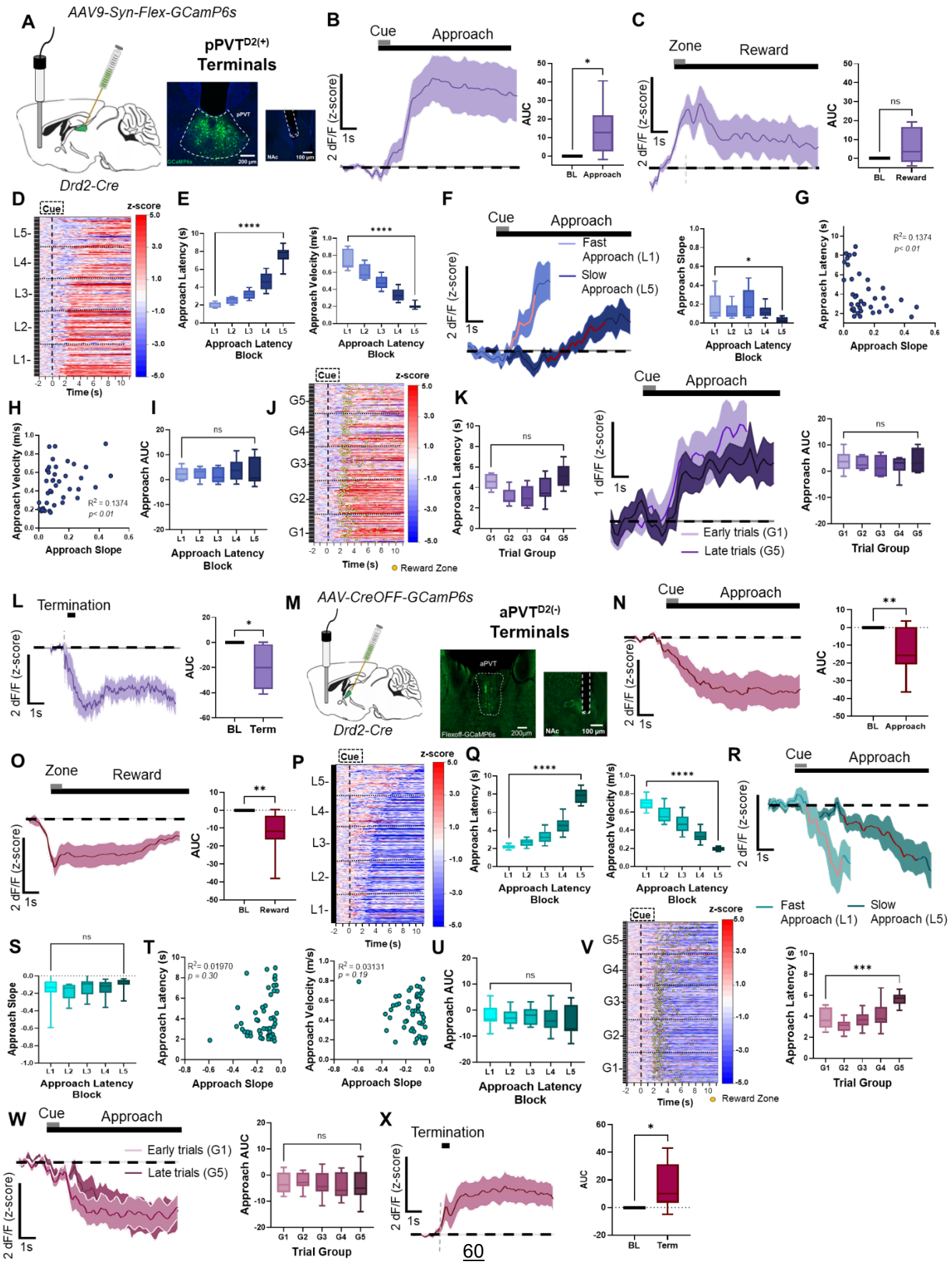

Supplement ary Figure 1

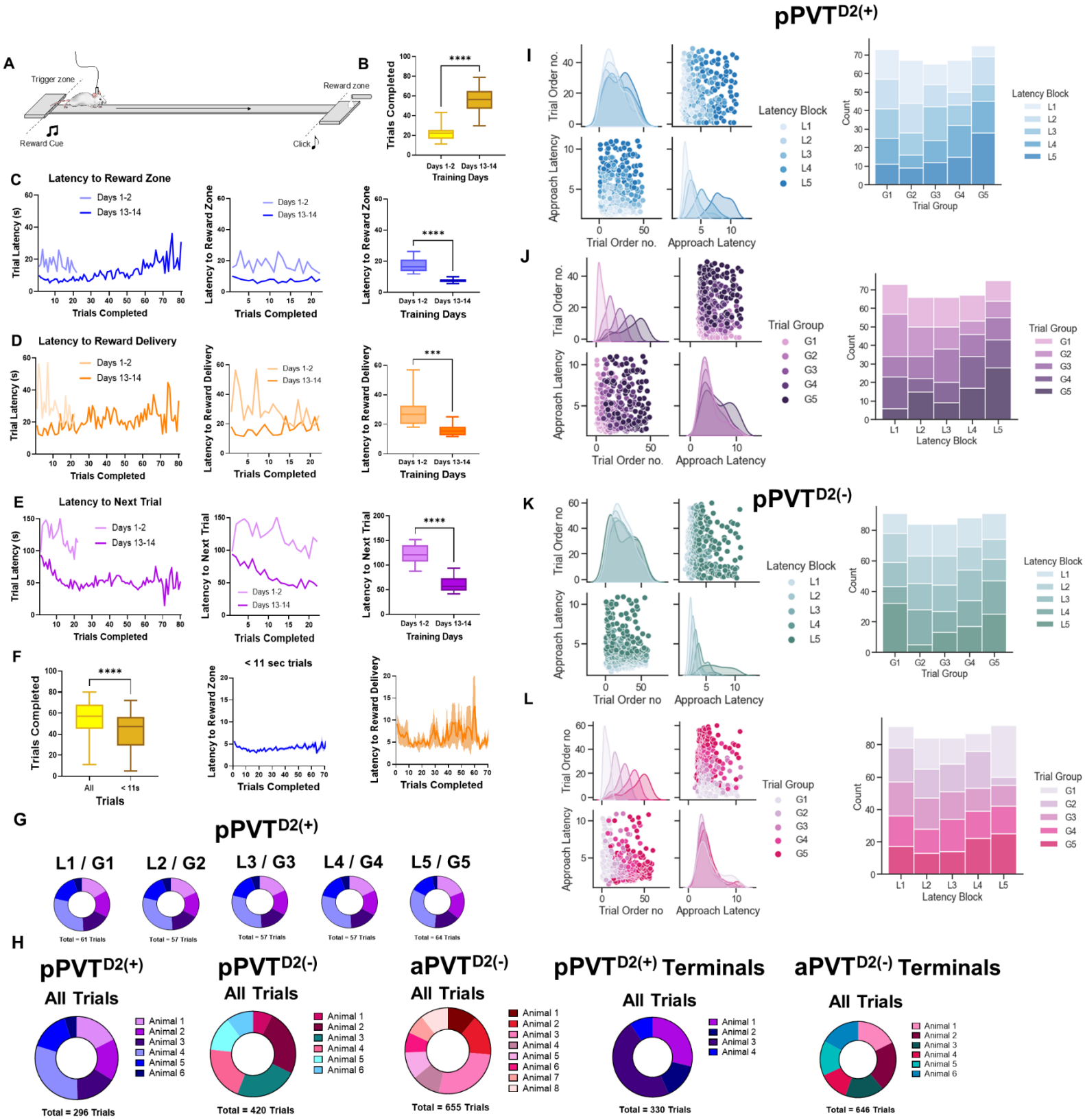

1331 Supplementary Figure 2

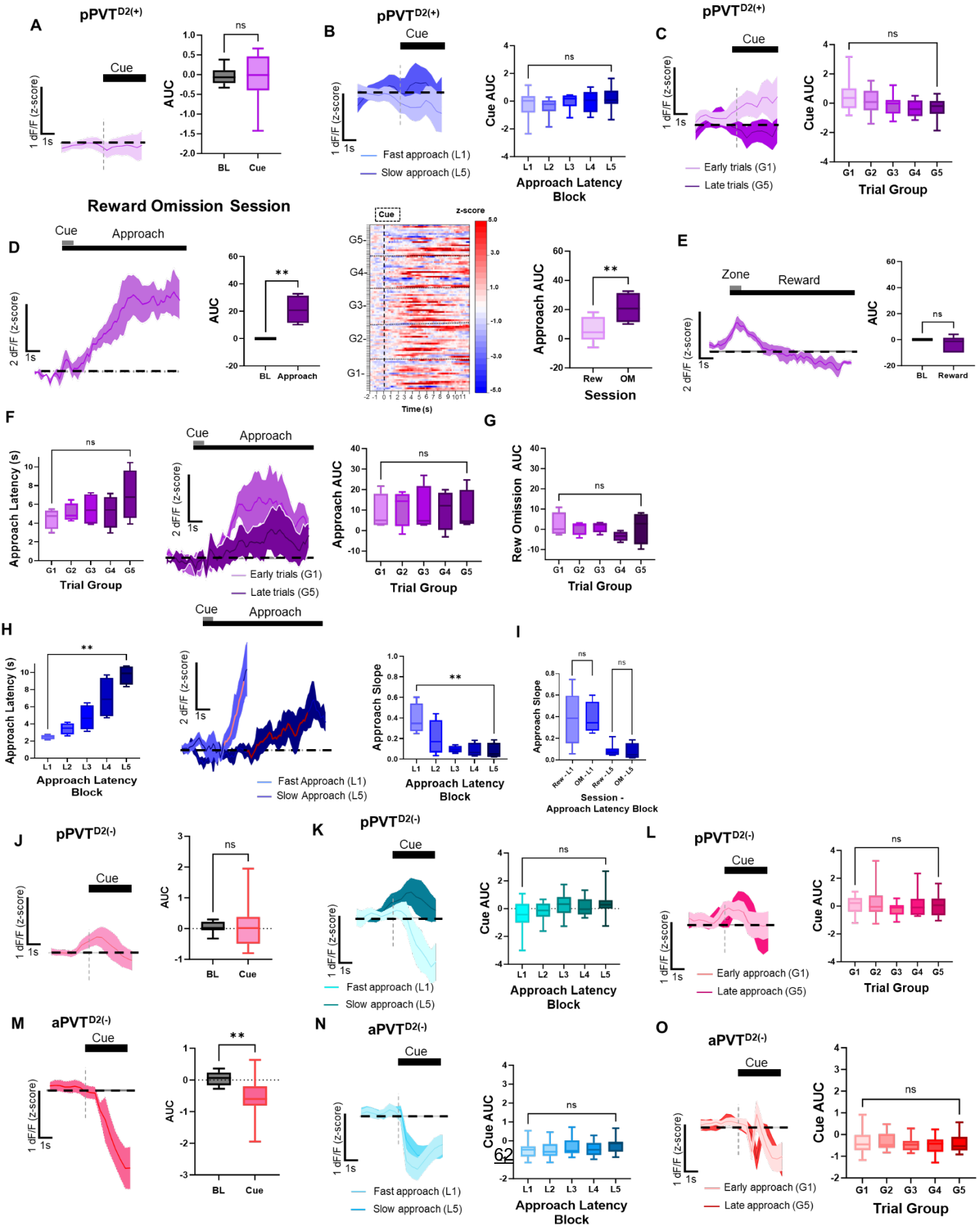

1332 Supplementary Figure 3

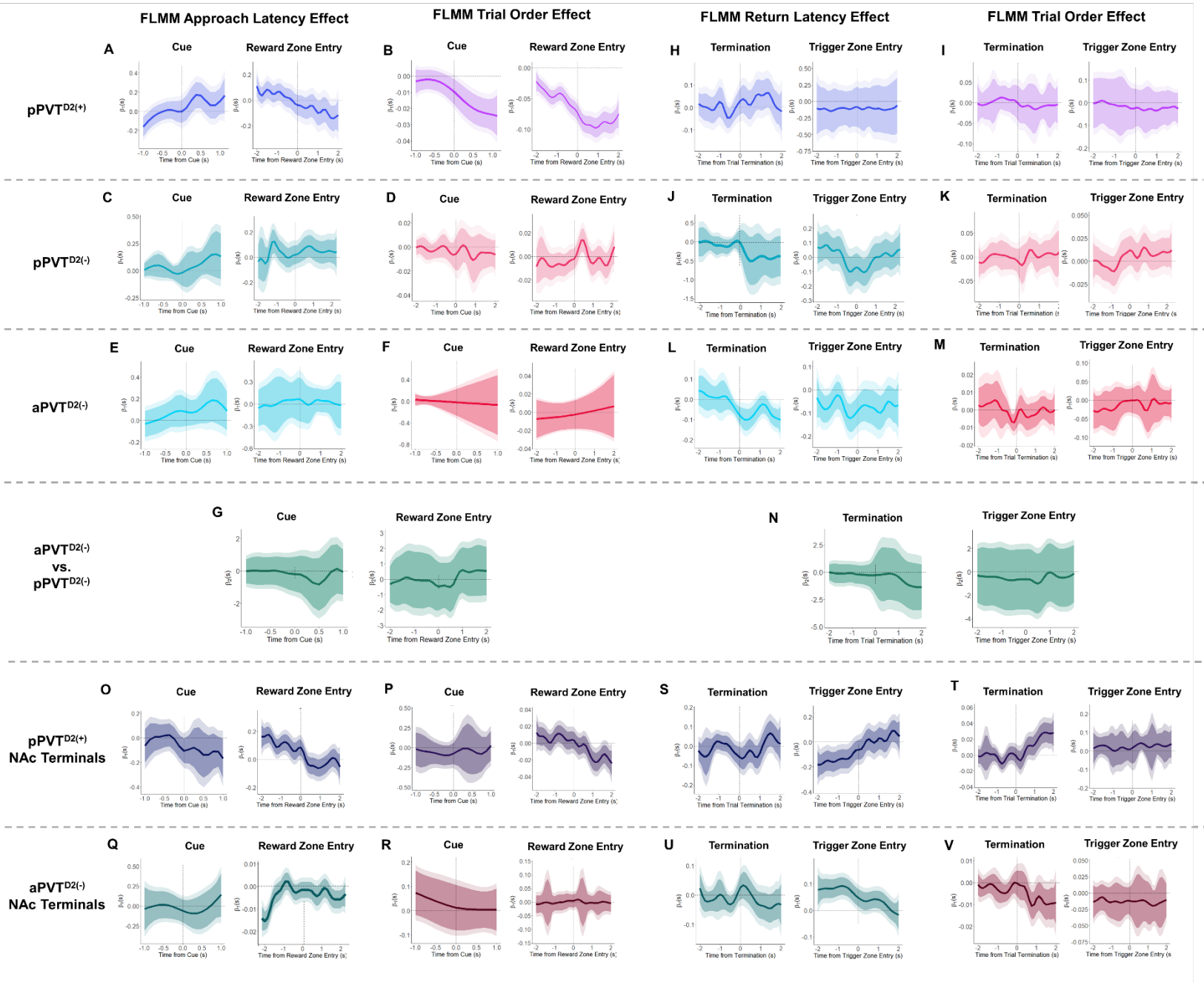
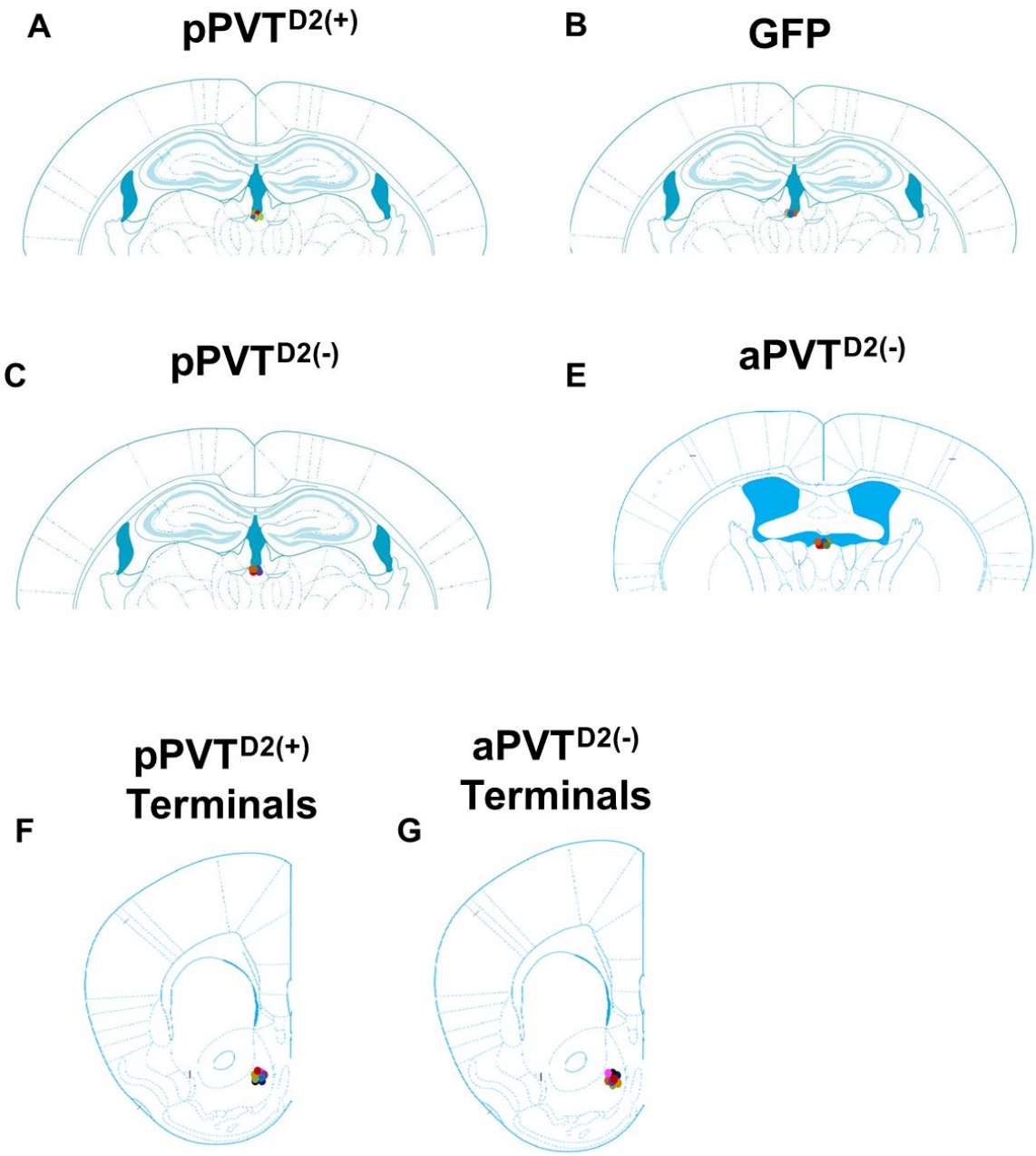
1333 Supplementary Figure 4